

Interfacial superconductivity in Cu/Cu₂O and its effect on shielding ambient electric fields[†]

Dale R. Harshman^{a,*} and Anthony T. Fiory^b

^a *Physikon Research Corporation, Lynden, WA 98264-9335, USA*

^b *Bell Labs Retired, Summit, NJ 07901-3437, USA*

(4 May 2025)

ABSTRACT

A model is presented for two-dimensional superconductivity at semiconductor-on-metal interfaces mediated by Coulomb interactions between electronically-active interface charges in the semiconductor and screening charges in the metal. The junction considered is native Cu₂O on Cu in which an interfacial double charge layer of areal density n , comprising superconducting holes in Cu₂O and mediating electrons in Cu, is induced in proportion to a sub-monolayer of adsorbed ⁴He atoms. Evidence for superconductivity on copper with prior air exposure is revealed in new analysis of previously published work function data. Based on a theory developed for layered superconductors, the intrinsic transition temperature $T_C = \beta n^{1/2}/\zeta$ is determined by n and transverse distance $\zeta \simeq 2.0 \text{ \AA}$ between the charge layers; $\beta = 1.933(6) e^2 \lambda_C/k_B = 1247.4(3.7) \text{ K-\AA}^2$ is a universal constant involving the reduced Compton wavelength of the electron λ_C . This model is applied to understanding the shielding of copper work-function patch and gravitational compression electric fields reported in the Witteborn-Fairbank gravitational electron free fall experiment. Interfacial superconductivity with $n \simeq 1.6 \times 10^{12} \text{ cm}^{-2}$, $T_C \simeq 7.9 \text{ K}$ and Berezinskiĭ-Kosterlitz-Thouless temperature $T_{\text{BKT}} \simeq 4.4 \text{ K}$ accounts for the shielding observed at temperature $T \simeq 4.2 \text{ K}$. Helium desorption and concomitant decreases in n and T_C replicate the temperature transition in ambient electric fields on falling electrons, as observed by Lockhart et al., and the vanishing of superconductivity above $T \simeq 4.8 \text{ K}$.

Keywords: 2D superconductor, Electron-mediation, Electron free fall,
Metal-semiconductor interfaces, Helium adsorption.

* Corresponding author.

E-mail address: drh@physikon.net (D.R. Harshman).

[†] Corrected preprint for D. R. Harshman and A. T. Fiory, *Physica C: Supercond. Applic.* 632 (2025) 1354600

doi: 10.1016/j.physc.2024.1354600

Corridendum on p. 20.

1. Introduction

Two-dimensional superconductivity is hosted in thin layers and at interfaces of differing materials, being notably bounded by crossovers to bosonic pairing at reduced carrier density and elevated sheet resistance [1-11]. Recalling previously-discussed possibilities for a condensed Bose gas in an electron surface layer [12], this work presents a model for two-dimensional superconductivity in a semiconductor interfaced with a metal and mediated by Coulomb interactions with screening charges. The pairing mechanism is electronic, yet differing from earlier concepts of superconducting surfaces [13,14] and interfaces [3,15-20], and is based on interlayer Coulomb-mediation initially introduced for high- T_C superconductivity [21]. While such an interfacial superconductive state portends intriguing materials physics, experimental data are available for testing the particular case of metallic Cu coated with its native oxide, forming a Cu/Cu₂O interface on the surface [22-24]. Evidence for superconductivity on previously air-exposed copper is manifested in a jump in the thermally-modulated work function, observed to be similar in magnitude to superconducting niobium (see Section 3.1). Surface superconductivity provides a plausible and quantifiable explanation for the shielding of ambient electric fields arising from work-function patch effects [25] and differential gravitational compression (DMRT field [26-29]) inside the copper tube held at 4.2 K in the electron gravitational drift measurements of Witteborn and Fairbank [30,31]. Copper-coated electrode plates in magnetic field levitation apparatus operating at liquid helium temperatures have also conveyed no evidence of patch-effect electric fields in contrast to a titanium coating [32,33].

Adsorption of ⁴He atoms, presumed to be in trace quantities, appears to be essential for producing these unique-to-copper effects. This interpretation follows from the resemblance of the temperature dependence of the ambient electric field reported by Lockhart et al. [34] to that of the Cu work function in ⁴He gas [35], as noted in an early review [36]. Quantitative analysis of these effects is presented in the experimental Section 3. It is, therefore, proposed herein that the Cu/Cu₂O interface junction is charged by a sub-monolayer of adsorbed ⁴He atoms. Strong electron repulsion by ⁴He, effectively pushing electron charge towards the copper, induces a double charge layer at the interface, comprising positively charged holes in semiconducting Cu₂O and negatively charged screening charges in the Cu. These charges form in equal numbers as a consequence of electrical neutrality of the ⁴He ad-atoms.

A schematic drawing of the theoretical Cu/Cu₂O structure is given in Fig. 1, which includes the adsorbed ⁴He atoms. Valence band holes in Cu₂O form a 2D

superconductor mediated by their Coulomb interactions with the screening charges in the Cu. Image-potential band-gap narrowing at the interface [16,18,19,37] may also contribute to stabilizing the 2D hole layer. As previously shown for thin-film and atomic layer structures [38,39], pairing arises from interlayer Coulomb interactions between electronic charges in adjacent superconducting and mediating layers, where optimization of the superconductive state is identified with a balance of charges between the two layers [21], taken as inherent for Cu/Cu₂O.

Witteborn and Fairbank measured time-of-flight distributions for electrons emitted upward along the axis of a vertical copper drift tube in vacuum for various values of applied electric field, introduced by passing a d.c. current along the tube [30,31]. The results give an ambient vertical electric field magnitude of $(0.02 \pm 0.09) m_e g/e$, where m_e is the electron rest mass and which is consistent with cancellation of gravity by the Schiff-Barnhill effect of gravitational sag in copper electrons [40]. Speculative explanations were offered for the evidently complete shielding of the much larger ($>10^3 m_e g/e$) patch and DMRT electric fields [41,42]. Notably, theoretical calculations of shielding by metallic surface layers fall 1 to 2 orders of magnitude short of the experimental observation [12,43], with the possible exception of a condensed Bose gas comprising paired charges [12]. The Cu/Cu₂O interface is more likely to provide the minimum materials disorder for enabling 2D superconductivity [44], when compared to the exposed surface considered by Bardeen [43], owing to hydrocarbons, bound hydroxyl, water, and possibly cupric products, e.g., CuO [22,23] and reflecting earlier concerns [12,45]. Moreover, superconductivity in Cu₂O benefits from high hole mobility ($>10^4 \text{ cm}^2\text{V}^{-1}\text{s}^{-1}$) at low temperature [46].

A metallic layer in the superconducting state could provide the observed shielding for an electron transiting the copper tube at 4.2 K, provided that this is below the temperature of the Berezinskiĭ-Kosterlitz-Thouless (BKT)

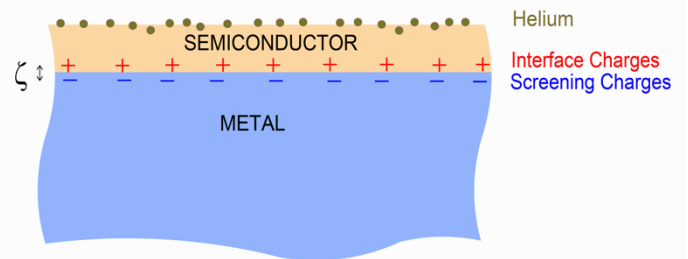


Fig. 1. Cross sectional view of the superconductor model structure of a semiconductor layer on a metal with adsorbed ⁴He atoms on the free surface, charges (+) in the semiconductor at the interface, screening charges (-) in the metal at the interface, and transverse separation distance ζ between the two types of charges.

transition T_{BKT} [47-50], a temperature generally falling below the intrinsic transition temperature T_C defined by a vanishing energy gap $\Delta(T_C) = 0$. Theoretical interfacial superconductivity is introduced for Cu/Cu₂O by the interaction between holes in the Cu₂O and Cu electrons with $T_C = \beta/\ell\zeta$ from earlier work [21]. Here $n \equiv \ell^{-2}$ is the area density of the superconducting charges, ζ shown in Fig. 1 is the transverse distance between the superconducting and screening charges, and $\beta = 1.933(6) e^2 \lambda_C/k_B = 1247.4(3.7) \text{ K}\cdot\text{\AA}^2$ is a universal constant, where $\lambda_C = \hbar/m_e c$ is the reduced Compton wavelength of the electron and k_B is the Boltzmann constant.

The density n of mobile holes, hence superconducting carriers, is assumed to be a fraction f_s of the density of adsorbed ⁴He atoms, which obeys the thermally activated log-pressure law [51] and rapidly desorbs as temperatures are raised above 4.2 K. Modeling the temperature-dependent ambient electric field data in Section 3 yields $f_s \sim 0.06$. Parameter values at $T = 4.2 \text{ K}$ are a ⁴He fractional monolayer $\theta \simeq 0.034$, $n \simeq 1.6 \times 10^{12} \text{ cm}^{-2}$, $T_C \simeq 7.9 \text{ K}$, and $T_{\text{BKT}} \simeq 4.4 \text{ K}$. Magnitudes of these parameters decrease at elevated temperatures, leading to the vanishing of superconductivity above $T \simeq 4.8 \text{ K}$. A non-negligible sub-monolayer of adsorbed ⁴He in the original work [30,31] may be surmised from the rather modest 80 L/s capacity of the ion pump, the protocol of not using the pump during data acquisition [41], and observations of ⁴He adsorption on copper at 4.2 K at pressures as low as $2 \times 10^{-11} \text{ Torr}$ [52]. Although the temperature-dependence data were taken with a ⁴He gas leak (see Ref. [34:Erratum]), examination of ⁴He-electron scattering in Section 3.3 finds that the published ambient field data have plausible magnitudes. As discussed in Section 2.2 with application to data analysis in Section 3.4, the interfacial superconductor yields negligible shielding of electric fields from applied currents in the copper tube as well as external magnetic fields. These attributes are consistent with the null or at best inconclusive tests for superconductivity conducted with conventional macroscopic probes [45,53].

In Section 2, properties of the electronic structure are developed, coupled with Coulomb mediation, 2D superconductivity, and electrostatic screening effects. Section 3 presents analyses of experiments concerning evidence for superconductivity on copper, adsorption of ⁴He gas on copper, and temperature-dependent ambient electric fields observed for free-fall electrons. Section 4 offers discussions of key issues, followed by the Conclusion in Section 5.

2. Theory

The concept of superconductivity arising from interactions between charges in an insulator or semiconductor and screening charges in an adjacent metal is unique, and has the potential for augmenting the scope

of interfacial superconductivity [3,11,44]. It follows as a direct extension of earlier theoretical work in which the genesis of unconventional superconductivity in certain layered compounds is non-phononic and vested in Coulomb interactions between charges occupying adjacent charge reservoirs [21]. The shielding of electric fields by such a thin superconducting charge layer, while certainly of general interest, can also provide a quantitatively plausible explanation for the enhanced electric field shielding effects observed in early electron gravitational drift measurements [30,31,34]. In Section 2.1, a model is constructed based on the theory described in Ref. [21] and the electric field screening effects are evaluated in Section 2.2.

2.1. Superconductive model

Interfacial band gap narrowing arising from screened image potentials [37,54] appears to be applicable for the Cu/Cu₂O interfaces, based on analysis of Schottky diodes that position the Fermi energy at almost midway in the Cu₂O band gap [55]. Image-potential raising of the valence band edge at the interface may be a factor in forming an interfacial potential well for holes in thin-film Cu-Cu₂O structures. A further consideration is whether band closure or metal-induced gap states (MIGS) occur at the interface [18,19,56], such as been observed for Cu/MgO [57], even though the 2.1-eV band gap of Cu₂O is comparatively smaller. A MIGS-based interfacial superconductor has also been proposed, based on the idea that pairing can be mediated by excitons in the semiconductor [19].

Several experimental studies searching for evidence of superconductivity [45,53] have recognized that shielding by a two-dimensional superconductor is limited by the critical temperature T_{BKT} [47-50], which from experiment [30] must be at least 4.2 K. Assuming disorder is a small perturbation, T_{BKT} scales with n/m^* for areal carrier density n and effective mass m^* and thus also with the Fermi energy $E_F = \pi \hbar^2 n/m^*$ as $T_{\text{BKT}} \sim 0.1 E_F/k_B$, approaching the theoretical limitation [4,8]. An order of magnitude estimate for $T_{\text{BKT}} \sim 4.2 \text{ K}$ is $n/m^* \sim 10^{12} \text{ cm}^{-2} m_e^{-1}$. Examination of the magnitude of n/m^* for a given model can therefore reveal whether superconductivity is thermodynamically stable. In their idealized electron layer on a copper surface, Hanni and Madey [12] found that shielding for $n = (4 \text{ to } 5) \times 10^{10} \text{ cm}^{-2}$ (with $m^* = m_e$) hypothetically supports superconductivity at $T_{\text{BKT}} \approx 0.1 \text{ K}$. The surface-state band on Cu₂O considered by Bardeen with hole concentration $n \approx 5 \times 10^{12} \text{ cm}^{-2}$ has a density-of-states $m^* \approx 170 m_e$ [43], yielding $n/m^* \approx 3 \times 10^{10} \text{ cm}^{-2} m_e^{-1}$ and $T_{\text{BKT}} \approx 0.1 \text{ K}$. Although the values of n/m^* derived in these quite different models for charge states on the surface appear to be too small by a factor of about 40, seemingly negating

the possibility of superconductivity, the magnitudes were designed to provide screening that replicates the ambient electric fields observed at temperatures above 4.2 K [34].

Adsorption of ^4He on the native oxide surface of Cu evidently induces n/m^* sufficient for superconductivity at 4.2 K, which is deduced in the following from the change in work function $\Delta W = -6$ meV measured at 4.2 K for an approximately monolayer coverage [35]. The sign of ΔW is opposite to the approximately +4 eV measured for ^4He adsorption on clean Cu [58], where electric dipoles oriented away from the surface develop at the adsorption sites [59-61]. Owing to strong electron repulsion, ^4He effectively pushes negative charge towards the metal [59,60], which is presumed to be the metallic side of the Cu/Cu₂O interface in the presence of native oxide. High Allen-scale ^4He electronegativity of 4.160, when compared to O (3.610), N (3.066), C (2.544), and Cu (1.85), expresses quantitatively this unique distinction of the full-shell valence electrons in ^4He . The double charge layers depicted in Fig. 1 follow from interpreting the observed negative ΔW as ^4He pushing some charge across the interface, promoting the formation of screening electrons in the Cu and a like number of hole carriers in the Cu₂O. The fractional charge per ^4He atom is found to be small ($f_s \approx 0.06$, Section 3.4) and thus entails small perturbations of pre-existing charges at the Cu-Cu₂O interface. In a rudimentary approach considering $-\Delta W$ as the shift in potential produced by filling a 2D electronic hole band, the free areal charge density $n = -\Delta W D$ for density of states $D = m^*/\pi\hbar^2$ yields $n/m^* = -\Delta W/\pi\hbar^2 = 2.75 \times 10^{12} \text{ cm}^{-2} m_e^{-1}$. This number is actually the lower bound on n/m^* , given that contributions to ΔW from outwardly oriented electric dipoles at the adsorption sites are unknown. However, the value shows compliance with the aforesaid criteria for minimum n/m^* , confirming that superconductivity with $T_{\text{BKT}} \gtrsim 4.2$ K is plausible. One may note that the magnitude of ΔW is on the order of 0.1% of $W \approx 4.65$ eV for clean polycrystalline Cu [62]) and $\sim 1\%$ of the +0.5 eV increase upon exposure of clean Cu to a dry O₂-N₂ ambient [63]; an increase with oxidation is ascribed to the electronegativity of O [64].

Accepting that Bardeen's analysis yields the correct order of magnitude for n [43], the foregoing result predicts that m^* is on the order of m_e and thus comparable to a Cu₂O-band effective mass. A plausible value $m^* = 0.69m_e$ is that measured for upper valence band holes (Cu 3d levels) at low temperatures, which exhibit high mobility ($5 \times 10^4 \text{ cm}^2 \text{ V}^{-1} \text{ s}^{-1}$) in bulk crystals of Cu₂O [46]. For the transverse distance ζ in Fig. 1, the charges are taken to occupy two planes defined by the locations of interfacial Cu ions. Averaging the ionic positions reported in several theoretical structure calculations of Cu/Cu₂O interfaces [24,65,66] gives $\zeta = 2.0 \text{ \AA}$.

Simulations of oxidized Cu using an atomically sharp Cu(100)/Cu₂O(111) interface [24] find positive and negative relative charges up to about $\pm 0.2/e$ on Cu in one to two layers into the metal, indicating built-in charge densities of $\pm 10^{13}/e/\text{cm}^{-2}$ that are slightly net negative. Magnitudes of these localized charges are comparable to the surface charge on a metal induced near a test charge at distance $\zeta/2$, according to the idealized method of images. Estimating characteristic lengths of such a surface charge in linear response theory [67],¹ the centroid is located 0.7 \AA closer to the interface, relative to the edge of a uniform positive-charge background, and is of thickness $\approx 2.2 \text{ \AA}$. The negative charges idealized in Fig. 1 therefore have their genesis in the net negative charges on interfacial Cu atoms.

Superconductivity at surfaces and interfaces, mediated solely by electronic or excitonic coupling, has been explored theoretically for some time in various contexts [15-18,20,68]. Electronic superconductive pairing in a semiconductor adjoining a metal, based on Coulomb interactions with screening electrons formed in the metal [12], appears possible because the charge layers shown in Fig. 1 directly reflect the elementary structural unit of a high- T_C superconductor [21,39]. The theoretical intrinsic transition temperature is defined by,

$$T_C = \beta/\ell\zeta = k_B^{-1}(\Lambda/\ell)(e^2/\zeta), \quad (1)$$

where ℓ is determined by the areal density of superconducting charges $n \equiv \ell^{-2}$ and ζ is the perpendicular distance between the charge layers ($\beta = 1247.4(3.7) \text{ K}\cdot\text{\AA}^2$ and $\Lambda = 1.933(6) \lambda_C$). According to [21], optimization of the superconductive state requires balance between the two types of charges, which is intrinsically satisfied in this case.

For a two-dimensional superconductor, the topological phase transition temperature is given by $T_{\text{BKT}} = [c^2\hbar^2/16e^2k_B]/L_s = [1.961 \text{ cm}\cdot\text{K}]/L_s$, where L_s is the renormalized magnetic screening length at temperature T_{BKT} [50], and where $T_{\text{BKT}} < T_C$. Ambient electric field data [30,34] indicate $T_{\text{BKT}} \gtrsim 4.2$ K at $T \approx 4.2$ K, for which $L_s \lesssim 0.47 \text{ cm}$.

The ratio of L_s to the intrinsic sheet magnetic penetration depth $\Lambda_0(T_{\text{BKT}})$ defines the renormalization factor $\epsilon_C = L_s/\Lambda_0(T_{\text{BKT}})$, which is non-universal. The result $\epsilon_C = 1.2 \pm 0.1$ is obtained for superconducting films with high sheet resistance in Ref. [69] and is adopted here. A superconducting layer sheathing a copper tube of surface area 0.15 m^2 would comprise a mosaic of about 10^4

¹ As described by Bardeen, "These charges arise from a modification by the external field of the tail of the wave functions of the electrons extending into the vacuum" [43].

regions of area L_s^2 that could sustain long range phase coherence at zero applied current. Consequently, the possibility exists for such a sheath to shield the patch and gravitational stress electric fields generated internally in the copper, while also freely admitting externally applied electric fields.

Temperature dependence in the intrinsic (*i.e.* not renormalized) penetration depth, expressed functionally as $f(T/T_C) \equiv \Lambda_0(0)/\Lambda_0(T)$ [70], is accurately described by the two-fluid expression $f(T/T_C) = 1 - (T/T_C)^4$ applicable to strongly coupled superconductors [71]. The renormalized screening length at $T = T_{\text{BKT}}$ is thus expressed as $L_s = \varepsilon_C \Lambda_0(0)/f_C$, where $f_C \equiv f(T_{\text{BKT}}/T_C)$. Effects of disorder, considered as possible in Ref. [42], are taken into account by using the Ginzburg Landau form $\Lambda_0(0) = \Lambda_L(1 + 0.75 \xi_0/l)$ [70], where ξ_0 is the Pippard coherence distance, l is the transport mean free path, and $\Lambda_L = m^*c^2/2\pi n e^2$ is the London sheet magnetic penetration depth for carriers of effective mass m^* and areal density n . Circular energy contours are assumed, giving the expression,

$$T_{\text{BKT}} = \pi f_C n \hbar^2 (8\varepsilon_C m^* k_B)^{-1} (1 + 0.75 \xi_0/l)^{-1}. \quad (2)$$

For a clean superconductor with $l \gg \xi_0$, Eq. (2) predicts the scaling $T_{\text{BKT}} \propto n/m^*$ with a non-universal numerical factor. A prediction from Eq. (2) is that the ratio of T_{BKT} to the Fermi temperature $T_F = E_F/k_B$ is given by the expression,

$$T_{\text{BKT}} / T_F = f_C [8\varepsilon_C (1 + 0.75 \xi_0/l)]^{-1}, \quad (3)$$

which approaches the theoretical maximum $T_{\text{BKT}} / T_F \rightarrow 1/8\varepsilon_C$ in the limits $\xi_0/l \rightarrow 0$ and $f_C \rightarrow 1$. This upper bound originates from the universal jump in the renormalized superfluid density ρ_S at T_{BKT} [4,72].

The right side of Eq. (2) may be expressed in terms of the normal electrical sheet resistance $R_N = m^*v_F/ne^2l$, the zero-temperature energy gap $\Delta_0 = \hbar v_F/\pi \xi_0$, where v_F is the Fermi velocity, and the superconducting quantum resistance for pairs $R_Q = h/4e^2$ such that,

$$T_{\text{BKT}} = \pi f_C (4\varepsilon_C k_B)^{-1} (l/\xi_0 + 0.75)^{-1} (R_Q/R_N) \Delta_0. \quad (4)$$

It is recognized that the penetration depth in the ‘‘dirty limit’’ $l \ll \xi_0$ is appropriate for very thin films of metallic superconductors, owing to high R_N [73], giving $T_{\text{BKT}} \approx \pi f_C (4\varepsilon_C k_B)^{-1} (R_Q/R_N) \Delta_0$ in a form applicable to granular superconducting films [69]. Resistance R_Q roughly sets the demarcation in R_N between the superconducting and

insulating phases [44,74-76]. Granular films comprise discontinuous superconducting grains interconnected by Josephson tunneling through weak links [76] coupled by Josephson critical current $I_C(T) \propto \Delta(T)/R_N$ [77,78], where $I_C(T) \propto (T_C - T)^2$ for insulating links [79], giving $k_B T_{\text{BKT}} = I_C(T_{\text{BKT}})h/8\varepsilon_C e$ [78], assuming negligible corrections for capacitive charging [80]. Although R_N near R_Q is considered in the present case, the superconducting layer is treated as a continuous two-dimensional sheet, rather than granular, because native oxidation produces an interface that completely covers the original Cu surface.

The transition temperature enters in Eqs. (2) – (4) through the expression $\Delta_0 = \gamma k_B T_C$ for coupling parameter γ . A value for low carrier density may be estimated from the quasi-2D superconductor $\text{Li}_{0.011}\text{ZnNCl}$ [6] for which the tunneling gap $\Delta_0 = 4.50$ meV and intrinsic resistive $T_C = 20.1$ K work out to indicate strong coupling with $\gamma = 2.5$. Adopting this value here, the Pippard coherence distance $\xi_0 = \hbar v_F/\pi \gamma k_B T_C$ with Eq. (1) for T_C gives $\xi_0 = \gamma^{-1}(2/\pi)^{1/2} \hbar^2 \zeta/\beta k_B m^* = 65.6 \text{ \AA}$. Note that this expression for ξ_0 is independent of n , T_C , and R_N .

Denoting the reduced normal-state resistance as $r_N = R_N/R_Q$ and given by $r_N = 4(2\pi)^{-1/2}(\ell/l)$, the mean free path may be expressed as,

$$l = 4(2\pi)^{-1/2} \ell/r_N, \quad (5)$$

showing that the limitation $r_N \lesssim 1$ for superconductivity corresponds to $l \gtrsim 1.596 \ell$. The criterion $k_F l \gtrsim 1$ for a metallic normal state of Fermi wavevector $k_F = (2\pi)^{1/2}/\ell$ evaluates to $k_F l \gtrsim 4/r_N$, which is automatically satisfied for $r_N \lesssim 1$. Equation (5) is utilized by assuming that r_N is a materials constant independent of the quantity of adsorbed ^4He , which is rationalized by considering ^4He as both effectuating n as well as being dominant in carrier scattering. The screening charges function similarly to ultra-shallow ionized acceptors, yielding l scaling with ℓ at low temperature.

2.2. Effect of electrostatic fields

The following treats the function of the electron beam circuit as a current detector connected to the copper tube and thereby the superconducting surface layer. This emulates the electrical system of the apparatus [41], where the copper tube is resistively connected to the electron source and detector through external power supplies. Considering the case of zero current in the copper tube, the electrochemical potential in the superconductor is given to be nearly uniform and constant in time, supporting counter-flowing supercurrents that cancel electrostatic fields [81,82], including the DMRT and patch (surface-parallel component) electrostatic fields introduced by the

copper tube. Temperature gradients along the tube are presumed to be small enough for cancelling thermoelectric fields as well. As a consequence of the supercurrent being confined to a curved two-dimensional surface, components of electrostatic fields perpendicular to the tube surface remain unshielded.

Superconductivity is affected by small surface-normal components of the longitudinal magnetic field used for centering the electron flow along the tube axis [41]. Such locally transverse magnetic field components B_{\perp} , which arise from variations in magnitude and axial alignment [41], generate free supercurrent vortices (magnetic flux quanta) with densities and both senses of circulation changing sinusoidally around the circumference of the tube. Guided by planned magnetic field variations up to 0.1 G [41] and for B_{\perp} assumed to be within ± 0.05 G, the average free vortex density is $n_f = (1/2)B_{\perp}/\phi_0 \approx 10^5 \text{ cm}^{-2}$, where ϕ_0 is the superconducting flux quantum, corresponding to $N_v \approx 10^8$ vortices in the superconductor (a cylinder of diameter $d_T = 5$ cm and length $h = 90$ cm [41]). Free vortices in a superconductor are generally held stationary by pinning at defects (e.g., related to the copper surface texture [41]), thereby keeping the superconducting phase invariant with time. Temperature gradients along the tube are presumed to be sufficiently small so as to maintain zero magneto-thermoelectric voltages in the pinned vortex state [83,84]. Thus, the screening effect associated with the superconductivity is time invariant.

Exceptions to pinned vortices occur during flux flow driven by a transport current at temperatures very close to T_{BKT} , where thermally excited vortex-pairs screen the pinning centers, allowing the free vortices to produce flux flow resistance and dissipation [85]. From the Bardeen and Stephen theory of vortex motion [86], the sheet resistance is given by $R_f = 2\pi\xi^2 B_{\perp} R_N / \phi_0$, which evaluates to 0.014Ω by taking $\xi = 0.855 [\xi_0 / (1 - T_{\text{BKT}}/T_C)]^{1/2} = 135 \text{ \AA}$ from the ‘‘dirty’’ form [70]. The resistance of the superconducting cylinder may be approximated as $R = R_f h / \pi d_T = 0.08 \Omega$, which generates a Johnson-Nyquist noise voltage $V_{\text{rms}} = (4k_B T R / \Delta t)^{1/2}$. With $\Delta t \sim 1$ second as the transit time for the slowest electrons [41], one has $V_{\text{rms}} = 4 \times 10^{-12} \text{ V}$.

Microscopically, thermal noise originates from random vortex motion with diffusivity $D_v = \mu_v k_B T$ [50], as expressed terms of the vortex mobility $\mu_v = (R_N / R_O) \xi^2 / \hbar$ derived from R_f . At $T = 4.2$ K, $D_v = 0.80 \text{ cm}^2/\text{s}$. Diffusive displacement of a single vortex projected along the circumference of the cylinder changes the phase of the superconducting order parameter along its length by $\Delta\phi \sim (2D_v \Delta t)^{1/2} / \pi d_T \approx 0.5$ radian and, from the a.c. Josephson equation, a voltage noise increment of $V_v = (\hbar/2e) \Delta\phi / \Delta t \approx 2 \times 10^{-16} \text{ V}$. Average voltage noise created by N_v vortices is thus estimated from the standard deviation as $\pm N_v^{1/2} V_v \sim$

$\pm 2 \times 10^{-12} \text{ V}$, in essential agreement with V_{rms} . Vortex pinning emerges for $T < T_{\text{BKT}}$ as the number of thermally excited vortex pairs rapidly diminishes, decreasing the flux-flow resistance [85] and accordingly the thermal voltage noise. The above estimates are comparable to the total experimental noise, which is at least $0.09 \text{ mgh}/e \approx 5 \times 10^{-12} \text{ V}$, expressed as a voltage [30].

An applied electric field E_A is induced by passing an electric current longitudinally through the copper tube. According to specifications in Ref. [41], for example, $E_A = 10^{-10} \text{ V/m}$ is obtained with a current of $2 \times 10^{-4} \text{ A}$ through a tube of resistance $4.5 \times 10^{-7} \Omega$. Continuity of E_A across the copper-superconductor interface is maintained by the flux-flow resistive state. For $R \sim 0.08 \Omega$, the superconductor transports a fraction of at least 6×10^{-6} of the applied current, exclusive of an indeterminate vortex depinning current. The DMRT and patch fields are thermodynamically non-dissipative, e.g., the lattice compression field in the copper is largely shielded (factor $\sim 1/7$ [27]) by mobile electrons in the copper. Hence, these electrostatic fields neither invoke nor contribute to time dependence in the phase of the superconducting order parameter, such as flux-flow dissipation, in the presence of a transport current.

The ambient electric field E inside the copper tube (positive denoting the upward direction) is the sum of components:

$$E = E_G + S E_T + E_A, \quad (6)$$

where $E_G = -m_e g / e = -5.6 \times 10^{-11} \text{ V/m}$ is the gravitational sag field from mobile carriers [40], E_T is the sum of the gravitational and patch fields from the copper tube, S is the shielding factor, and E_A is the electric field applied to the copper tube. For mobile carriers in a normal 2D Fermi gas, the shielding factor is $S_N = (\partial\mu/\partial n) / 4\pi e^2 \zeta$ with chemical potential $\mu = k_B T \ln[\exp(\pi \hbar^2 n / m^* k_B T) - 1]$ [12]. Temperature dependence in S_N is given by,

$$S_N = (\hbar^2 / 4m^* e^2 \zeta) [1 - \exp(-\pi \hbar^2 n / m^* k_B T)], \quad (7)$$

where the coefficient sets the low-temperature limit as $S_N \rightarrow \hbar^2 / 4m^* e^2 \zeta = 0.096$. Normal excitations in the superconducting state are assumed to have the same S_N of Eq. (7) as in the normal state.

Superconductivity is introduced by using the two-fluid model with normal and superconducting shielding factors, denoted \tilde{S}_N and \tilde{S}_S , respectively. Drawing an analogy to parallel transport in the two-fluid model, superconductivity in the surface electron layer is constructed as a parallel

connection of two resistances, \tilde{R}_N and \tilde{R}_S , representing the normal and superconducting components, respectively, which are coupled to the copper tube by a series resistance R_C . For voltage drop V_T across the length of the copper tube and voltage drop V_{OUT} across the length of the surface electron layer, the ratio of the voltages gives the shielding factor as $S = V_{OUT}/V_T = [1 + R_C(\tilde{R}_N^{-1} + \tilde{R}_S^{-1})]^{-1}$. The normal shielding factor is obtained from S in the limit $R_S \rightarrow \infty$ as $\tilde{S}_N = (1 + R_C/\tilde{R}_N)^{-1}$ and the superconducting shielding factor in the limit $R_S \rightarrow 0$ as $\tilde{S}_S = \tilde{R}_S/R_C$. The shielding factor is thus obtained in terms of normal and superconducting components by the expression,

$$S = (\tilde{S}_N^{-1} + \tilde{S}_S^{-1})^{-1} = \tilde{S}_N / (1 + \tilde{S}_N/\tilde{S}_S). \quad (8)$$

In the normal state $T > T_C$, $S = S_N$ and $\tilde{S}_S = 1$, thereby determining $\tilde{S}_N = S_N/(1 - S_N)$ in terms of S_N in Eq. (7). In the fully coherent superconducting state, $\tilde{S}_S/\tilde{S}_N \ll 1$, yielding $S = \tilde{S}_S$. Minimum values of \tilde{S}_S in the superconducting state are possibly limited by finite critical currents and extrinsic disorder.

The ambient electric field in the presence of superconducting shielding thus evaluates to,

$$E = E_G + \tilde{S}_N E_T / (1 + \tilde{S}_N/\tilde{S}_S) + E_A. \quad (9)$$

The electronic gravitational sag field term E_G acts against gravity, irrespective of the presence of superconductivity [40]. The substances coating the copper tube are considered to have insufficient mass or mechanical rigidity for generating the theoretical DMRT field of a bulk insulator [28].

At temperatures $T > T_{BKT}$, the presence of superconducting fluctuations is assumed to yield partial shielding, such that in Eq. (9) one has $\tilde{S}_S^{-1} \propto \xi_+^2$, where ξ_+ is the order parameter correlation length. This assumes that \tilde{S}_N^{-1} scales in like manner as the fluctuation conductivity and transverse magnetic susceptibility, both of which vary as ξ_+^2 . For $T \gtrsim T_{BKT}$, $\xi_+^2 \propto \exp\{2[b\tau_C/(T/T_{BKT} - 1)]^{1/2}\}$, where b is a dimensionless parameter of order unity and $\tau_C = T_C/T_{BKT} - 1$ [50]. The maximum value taken by ξ_+ is limited to the lesser of L_s or the spacing between free vortices spawned by an external magnetic field. Using the interpolation formula for $T > T_{BKT}$ presented in Ref. [50], fluctuation shielding is approximated for temperatures up to T_C by,

$$\tilde{S}_S = S_1 b \sinh^{-2}\{[b\tau_C/(T/T_{BKT} - 1)]^{1/2}\} \quad (10)$$

(for $T_{BKT} < T < T_C$).

For $T \geq T_C$, solution of Eq. (10) for $\tilde{S}_S = 1$ establishes the value of the prefactor $S_1 = b^{-1} \sinh^2\{[b\tau_C/(T_C/T_{BKT} - 1)]^{1/2}\}$.

3. Experiment

Analyses of published experimental data for oxidized copper are presented in the following sub-sections, showing the evidence for superconductivity, a 2D electronic layer, and temperature-dependent superconductive shielding of ambient electric fields, while also quantitatively relating the experimental observations to ^4He adsorption.

3.1 Evidence for superconductivity

Work-function temperature-derivatives dW/dT vs. T for native-oxidized polycrystalline copper were reported by Free et al. [87]. Figure 2 shows data transcribed from Figs. 3 and 4 therein, which has extended temperature range compared to earlier works [35,88]; W is expressed in the experimental units of voltage. The study was intended to search for features that could be associated with a shielding transition [34], yet concluded that no anomalies were observed, e.g., at 4.2 or 4.5 K. However, the temperature dependence of dW/dT does indeed contain evidence of a discontinuity at the lower temperature of $T_X = 3.7$ K, as indicated by two solid red lines in Fig. 2 as described below. This feature is possibly related to the sharp change at approximately 4 K reported for the contact potential of copper in helium gas [89].

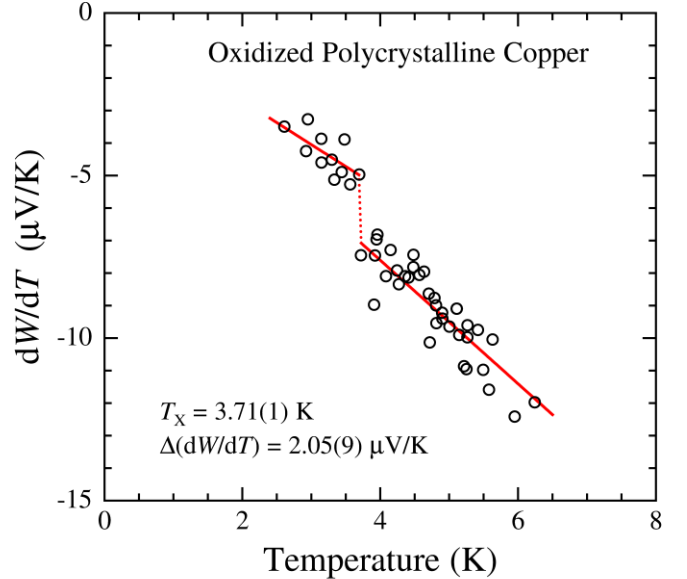


Fig. 2. Temperature derivative of the work function of copper with native oxide, dW/dT (symbols), vs. temperature [87]. Lines denote linear-in- T variations for $T < T_X$ and $T > T_X$ with jump $\Delta(dW/dT)$ indicated by dotted line at T_X . Values of parameters in legend.

The solid lines in Fig. 2 denote the function

$$dW/dT = w_1\theta_v(T_X - T)T + w_2\theta_v(T - T_X)T, \quad (11)$$

where θ_v is the unit step function; a dotted line marks the discontinuity. A three-parameter regression fit to the data, satisfying the thermodynamic limit of $dW/dT \rightarrow 0$ as $T \rightarrow 0$, yields slopes $w_1 = -1.35(6) \mu\text{V K}^{-2}$ and $w_2 = -1.90(2) \mu\text{V K}^{-2}$, $T_X = 3.71(1) \text{ K}$, an rms deviation with respect to the data of $0.616 \mu\text{V K}^{-1}$, and chi-square $\chi^2 = 0.380$ (for $\pm 1 \mu\text{V K}^{-1}$ intrinsic noise [87]). The jump $\Delta(dW/dT)$ at T_X is defined by the discontinuity as $(w_1 - w_2)T_X = 2.05(9) \mu\text{V K}^{-1}$. Division by the value $w_2T_X = -7.0(3) \mu\text{V K}^{-1}$ for dW/dT at T just above T_X yields the dimensionless normalized jump given by the quantity $w_1/w_2 - 1 = -0.29(3)$. Several continuously smooth functions through the origin are also tested for statistical comparison. Fitting a single continuous line more than doubles χ^2 to 1.027, while a smooth quadratic curve increases χ^2 to 0.629, from which F-test probabilities of 0.0006 and 0.048 [90] are, respectively, obtained. Existence of a jump in the data for dW/dT is therefore at least 95% probable, with its value resolved to better than 5% statistical accuracy.

This may be compared to results from work function data for Nb, where a jump in dW/dT of about $-5 \mu\text{V K}^{-1}$ for $T_C = 9.2 \text{ K}$ was reported [88]. With $dW/dT \approx 15 \mu\text{V K}^{-1}$ just above T_C , estimated from Fig. 5 in Ref. [88], the normalized jump for Nb is about -0.33 . Values of the normalized jump in dW/dT for Cu and Nb therefore have the same sign and nearly equal magnitudes within the experimental uncertainties. In the case of Nb, the jump at T_C is associated with superconductivity in Nb [88].

It has been suggested that the work function may be able to detect temperature dependent changes in the chemical potential μ at low electron density [91], particularly the jump in $d\mu/dT$ at T_C that is derived in three-dimensional models [91]. While the behavior of μ in 2D and 3D may be similar [1,92], the signature feature of the superconducting transition in 2D generally occurs in the renormalized superfluid density ρ_s . Theory predicts a square-root singularity and discontinuity in ρ_s at T_{KBT} [50,72], which is observed to be continuous in temperature at finite frequency [85]. How such properties are reflected in measurements of dW/dT remains an open question.

An electronic surface layer on the oxidized Cu may be assumed [12], since the measured magnitudes of dW/dT are 50–100 times larger than estimates for bulk Cu and ~ 30 times larger than the measured thermopower of the sample [87]. As a surface probe, the work function is specific to electronic charge and presumably insensitive to mass or spin, hence it is logical to identify T_X as an actual

measurement of $T_{\text{BKT}} = 3.70(2) \text{ K}$. With parameters $m^* = 0.69m_e$, $\zeta = 2.0 \text{ \AA}$, $r_N = 1.0$, and $\varepsilon_C = 1.2$ from Section 2.1, one obtains 2D carrier density $n = 1.29(1) \times 10^{12} \text{ cm}^{-2}$ and $T_C = 7.08(2) \text{ K}$ at T_X . Other derived parameters with values at T_X are $k_F\xi_0 = 1.86(1)$ and Fermi temperature $T_F = 52 \text{ K}$, the latter yielding $T_{\text{BKT}}/T_F = 0.071$. Although care was taken in Ref. [87] to avoid introducing helium, vacuum pressure is not specified ($P = 10^{-7} \text{ Torr}$ is stated for the Nb experiment [88]). A small sub-monolayer of ^4He is therefore consistent with an unavoidable level of contamination as originally conjectured for high vacuum [31],² estimated from data analyses in Sections 3.2 and 3.4 to be 0.025 fractional ^4He monolayer at 3.7 K.

The jump in the temperature dependence of the work function derivative dW/dT measured for copper [87] is therefore considered to be significant evidence for a 2D superconducting transition on Cu. Interpretation of the jump's magnitude awaits further theoretical development, in particular for the temperature dependence in the chemical potential $\mu(T)$ in 2D. A jump in $\mu(T)$ at T_C is derived for 3D models of low electron density superconductors, e.g. a magnitude of $\Delta_0^2/4T_C\mu_N(T_C)$, where $\mu_N(T_C)$ is the normal-state chemical potential at T_C [91].

Temperature linearity in dW/dT for $T < T_X$ points to the presence of a non-superconducting metallic phase on the surface, possibly as a coexisting bosonic metal [5,7,10,11]. However, the metallic signature may simply reflect sensitivity to the Cu substrate and the screening charges. Other possibilities are the surface states on Cu_2O considered by Bardeen [43] and/or surface charges [12,42], which could account for the linear-like behavior noted for the temperature dependence of ambient electric fields for $T > 4.2 \text{ K}$ [12,43].

3.2. Adsorption of ^4He on copper

De Waele et al. [35] report that exposure of a Cu sample to helium (^4He) gas reduces the work function W and present results (in units of voltage) for the temperature dependence of the change relative to 4.2 K, denoted as $W_T - W_{4.2}$. A digitized replica of the curve in Fig. 9 therein is shown as the solid curve in Fig. 3. A He leak produces a similar effect on the work function of Nb, indicated by comparable temperature derivatives dW/dT at 4.2 K, i.e. $\sim 3 \text{ mV/K}$ for Cu and 1.6 mV/K for Nb [35]. Absent the admitted helium gas, results for dW/dT have substantially smaller magnitudes ($\sim 1\%$): $-(8 \text{ to } 10) \mu\text{V/K}$ for Cu [35,87] and $+(8 \text{ to } 13) \mu\text{V/K}$ for Nb [35,88]. The following analysis considers the published drawing as accurately representing the data.

² See Ref. [31] (p. 1050), "A possible mechanism for this is adsorption of hydrogen and helium from the background gas during cooling." The concentration of ^4He in air is 5.2 ppm.

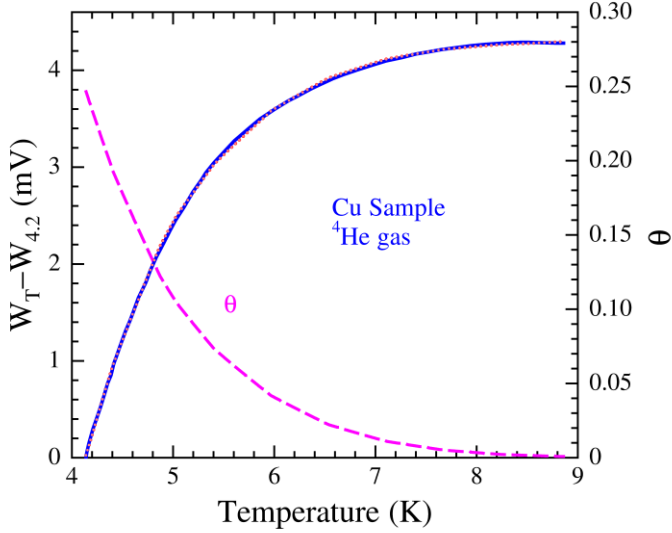


Fig. 3. Temperature dependence of the work function change $W_T - W_{4.2}$ for a copper sample in ^4He gas (solid curve) [35] and model function (dotted curve). Curve θ (dashed, right scale) is the modeled fractional ^4He gas coverage determined from Eq. (14).

The dotted curve in Fig. 3 is a function that scales $W_T - W_{4.2}$ with the fraction of ^4He monolayer coverage θ [93] such that,

$$W_T - W_{4.2} = \Delta W + W_1 \theta, \quad (12)$$

where ΔW is the maximum work function change and W_1 (< 0) is the rate of work function change per unit θ . As reported in Ref. [35], the change in W saturates at 6 mV for $\theta \sim 1$, which corresponds to a ^4He areal density of about $7.9 \times 10^{14} \text{ cm}^{-2}$ [94]. Theory for θ is based on the log-pressure expression derived for gas adsorption on a flat surface [51],

$$\theta = \ln \left\{ \frac{(U_b/k_B T)}{\ln[P/P_{\text{vap}}(T)]} \right\}, \quad (13)$$

where U_b is the binding energy ($U_b < 0$), P is the pressure, and $P_{\text{vap}}(T)$ is the saturated vapor pressure at temperature T or the critical pressure of ^4He for $T > 5.2 \text{ K}$.

Reported theoretical values of U_b for ^4He on Cu are in the range $-(3.55 \text{ to } 6.79) \text{ meV}$ [59,61,95,96]. More relevant, however, are results for ^4He adsorption on Cu samples with similar ambient exposures prior to study. For example, isosteric heats of adsorption Q_{st} derived from adsorption isotherms markedly deviate from a constant, increasing from 6.6 meV at $\theta \approx 1$ to about 12 to 15 meV for $\theta \rightarrow 0$, which is indicative of inhomogeneous

adsorption of ^4He on Cu [94]. The limit $\theta \rightarrow 0$ suggests $U_b \sim -(10 \text{ to } 14) \text{ meV}$, which is consistent, within experimental uncertainty, with $U_b = -15.2 \text{ meV}$ deduced independently by a time-of-flight diffusion method [97,98].

Inhomogeneous absorption is taken into account by assuming a Gaussian distribution in U_b , where the mean U_{b0} and standard deviation σ_b are treated as adjustable parameters, giving,

$$\theta = \pi^{-1/2} \sigma_b^{-1} \int_{-\infty}^{U_T} \exp \left[-0.5 (U - U_{b0})^2 / \sigma_b^2 \right] \times \ln \left\{ \frac{(U/k_B T)}{\ln[P/P_{\text{vap}}(T)]} \right\} dU + \theta_0, \quad (14)$$

where $U_T = \ln[P/P_{\text{vap}}(T)]k_B T$ and the constant θ_0 is added for general application (Section 3.4). Since the experimental pressure is not given, the function of Eq. (12) is illustrated with $P = 2 \times 10^{-5} \text{ Torr}$ (twice the experimental base pressure) and setting $\theta_0 = 0$. Parameters obtained from chi-square minimization are $\Delta W = 4.306(2) \text{ mV}$, $W_1 = -17.37(8) \text{ mV}$, $U_{b0} = -7.60(2) \text{ meV}$, and $\sigma_b = 2.84(1) \text{ meV}$, yielding a 0.0163 mV rms deviation with respect to the data replica. Fitted functions are shown in Fig. 3, where $W_T - W_{4.2}$ is the dotted curve and θ is the dashed curve. The chi-square is weakly dependent on the choice of P over the range 10^{-9} – 10^{-2} Torr , owing to its strong correlation with parameter U_{b0} . For example, the frequently occurring pressure $P = 8 \times 10^{-9} \text{ Torr}$ reported by Lockhart et al. [34:Erratum] gives $\Delta W = 4.315(2) \text{ mV}$, $W_1 = -26.58(8) \text{ mV}$, $U_{b0} = -8.96(2) \text{ meV}$, $\sigma_b = 4.69(1) \text{ meV}$, and 0.0162 mV rms deviation. At $T = 4.2 \text{ K}$, the values of θ are 0.25 and 0.16 at $P = 2 \times 10^{-5}$ and $8 \times 10^{-9} \text{ Torr}$, respectively.

3.3. Ambient electric field measurement

Experimental methods in the electron-free fall experiments are described in Refs. [30,34], and [41] for measuring the force F on an electron transiting the copper tube by modeling time of flight spectra for electrons emitted from a pulsed source. Analytical functions are based on the Newtonian energy $W_F = F^2 t^2 / 8m + mh^2 / 2t^2 + Fh/2$ pertaining to an electron of initial energy W_F with transit time t and traversal distance h , and treating F as a fitting parameter [41]. Power-law exponents are used to parameterize the distributions in the electron emission energies and times of delay in traps, together with normalization and background noise parameters [41]. A theoretical maximum in time $t_{\text{max}} = (2hm/F)^{1/2}$ at minimum $W_F = Fh$ occurs for F opposing the upward flux of electrons. The ambient force on the electrons was obtained by measuring F with applied electric fields and extrapolating to zero field.

In [30], the negative ambient electric field of about -5×10^{-10} V/m at 4.2 K, observed with vacuum pressure below 4×10^{-10} Torr [30], has been argued as correct and unaffected by ^4He gas scattering [34:Erratum]. Validation that this is the case is the force $F = 1.3 \times 10^{-10}$ eV/m obtained from time of flight distributions in Ref. [31]. The analysis of electron flight times given below makes use of the experimentally verified electron- ^4He scattering cross section $\sigma_{e\text{-He}}$ at low energy [99], which is smaller by a factor of 2.5×10^{-4} than the theoretical value employed in Ref. [41]. Contrary to the negating conclusions and opinions expressed previously (see, e.g., Refs. [36] and [34:Erratum]), electron- ^4He scattering proves not to be a valid rationale for retracting the experimental ambient electric fields measured for $T > 4.2$ K.

3.3.1. Experimental errors

Scattering of the electrons by ambient ^4He gas has been presumed in Ref. [34:Erratum] to affect some of the results for F in Ref. [34], although perturbations from gas scattering on time of flight spectra [36] have not previously been explicitly included in analyzing the data. However, errors may be discerned by comparing data from the original experiments (Fig. 2 in Ref. [30]) with claimed gas pressure P well below 10^{-10} Torr [34:Erratum] and the heated tube experiments at 4.2 K with $P < 4 \times 10^{-8}$ Torr [34:Erratum] (Fig. 8a in Ref. [100]). The results for the absolute values of F at 4.2 K are combined and plotted against applied electric field E_A in Fig. 4. A solid diagonal line denotes the expression $|F| = |eE_A|$ for zero ambient force. Dotted curves denote the limits of uncertainty for the ambient force, given as $(0.13 \pm 0.51) \times 10^{-11}$ eV/m from statistical analysis of 11 data sets with $|E_A| < 2.5 \times 10^{-10}$ V/m, representing $|F| = |eE_A| \pm 0.09 m_{e,g}$ [30]. Most of these 11 data points in Fig. 4 are within or near the limits, while several appear to be significant outliers.

The diagonal line in Fig. 4 can essentially be employed as a reference from which deviations from unity of the ratios $r_F \equiv |F/eE_A|$ and $r_{t_{\max}} = r_F^{-1/2}$ provide indications of experimental errors. The 16 data points from Ref. [30] (“WF”) exhibit ranges $r_F = 0.24 - 1.42$ and $r_{t_{\max}} = 0.84 - 2.03$; statistics (mean \pm standard deviation) are $r_F = 0.98 \pm 0.30$ and $r_{t_{\max}} = 1.07 \pm 0.28$. For the 4 data points from Ref. [100] (“LWF”), the ranges are $r_F = 0.59$ to 1.48 and $r_{t_{\max}} = 0.82$ to 1.30 with statistics $r_F = 0.85 \pm 0.42$ and $r_{t_{\max}} = 1.14 \pm 0.22$. Accuracy of the results for F in experiments with the heated tube at 4.2 K thus appears to be about $\pm (40 \text{ to } 50) \%$, falling outside the experimental error bars of $\pm (15 \text{ to } 26) \%$. Deviations from the diagonal line also suggest systematic underestimations as $|F| \sim 0.6 |eE_A|$ at the highest applied electric fields $E_A \sim 10^{-7}$ V/m. At elevated tube temperatures of 4.3 to 11 K, ambient electric fields values of $E \sim 10^{-8}$ to $\sim 10^{-6}$ V/m are assigned

$\pm (23 \text{ to } 53) \%$ errors (Fig. 3 of Ref. [100]), which, in view of the above, are evidently realistic.

Systematic error from gas scattering at a given pressure diminishes with increasing F , as the electrons traverse the drift tube with increasing velocities. The induced electric dipole model for electron- ^4He scattering derived in Ref. [41], evaluated for $P = 4 \times 10^{-8}$ Torr and interaction energy $Fh \approx 10^{-7}$ eV, gives a scattering cross section $\sigma_{e\text{-He}} = 2 \times 10^{-16}$ m² and a scattering time $\tau_s = 0.04 t_{\max}$ at 4.2 K. Such analysis portends significant scattering of the electron beam (see, e.g., Refs. [36] and [34:Erratum]) which, in retrospect, was too conservative in view of the directly measured $\sigma_{e\text{-He}} = 5 \times 10^{-20}$ m² for low energy electrons [99]. At the highest ambient pressure of 4×10^{-8} Torr considered possible for a small ^4He gas leak in Ref. [34:Erratum], ambient fields are therefore reliably obtained for values larger than about 10^{-9} V/m in the heated tube experiment [34,100], which is substantially less than the 7.4×10^{-6} V/m criterion cited in Ref. [34:Erratum]. The corrected criterion limits observable perturbations by ^4He gas scattering to data obtained for temperatures near 4.2 K in Refs. [34] and [100].

A significant source of systematic error is the distribution in emission time delays in traps at the electron source, which smear out the cut-offs in the time of flight spectra at t_{\max} [30,41]. Trapping of the electrons prior to their entering the drift tube increases difficulty in data

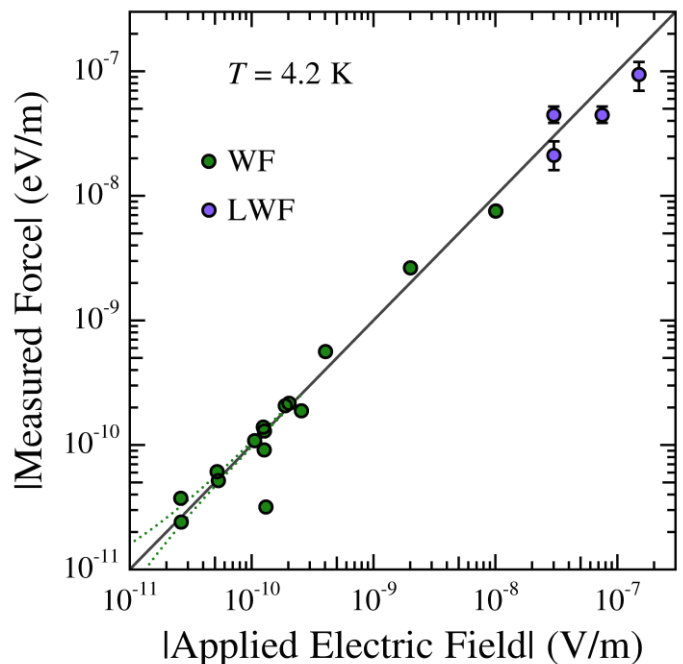


Fig. 4. Measured force on free-fall electrons vs. applied electric field (absolute values) at temperature $T = 4.2$ K from Refs. [30] (WF) and [100] (LWF). Solid line indicates zero ambient force; dotted curves denote ranges of statistical uncertainty obtained in Ref. [30].

analysis at the larger values of F used in experiments at the elevated drift-tube temperatures [100]. For tube temperatures of 77 and 300 K, results for ambient electric fields were derived from observed changes in intensities of detected electrons with applied electric fields [34,43,100]. Peculiarity in the field dependence, noted for data taken at 300 K in Ref. [42], is considered below for estimating the uncertainty in the reported ambient field.

3.3.2. 300 K data analysis

An effective ambient electric field of $E = (7.5 \pm 6) \times 10^{-6}$ V/m was measured for the drift tube at 300 K by applying electric fields of magnitudes significantly greater than E [34]. Variation in the relative intensity of detected electrons with applied force F_A is shown in Fig. 5 on linear scales, which transcribe data and trend curves in the original semi-logarithmic plots (see Fig. 7 of Ref. [100]). A dashed line (slope = $0.0116 \mu\text{V}^{-1}\text{m}$) illustrates the linear trend pointed out in Ref. [42]. The dotted curve is an estimated trend that is drawn from the experimental description presented in Ref. [34], where the number of detected electrons emitted at energies less than W is determined to be proportional to W itself. The relative intensity can be conjectured from the time of flight expression $W = F^2 t^2 / 8m + mh^2 / 2t^2 + Fh/2$ as the ratio I_r of W for $F = F_0 + F_A$ to its value at $F_A = 0$, where F_0 is the ambient force ($-eE$) and F_A is the applied force ($-eE_A$). This ratio is approximately represented as,

$$I_r = 1 + F_A h/2W_0 + (F_0 + F_A)^2 h^2 / 8W_0(2W_0 - F_0 h), \quad (15)$$

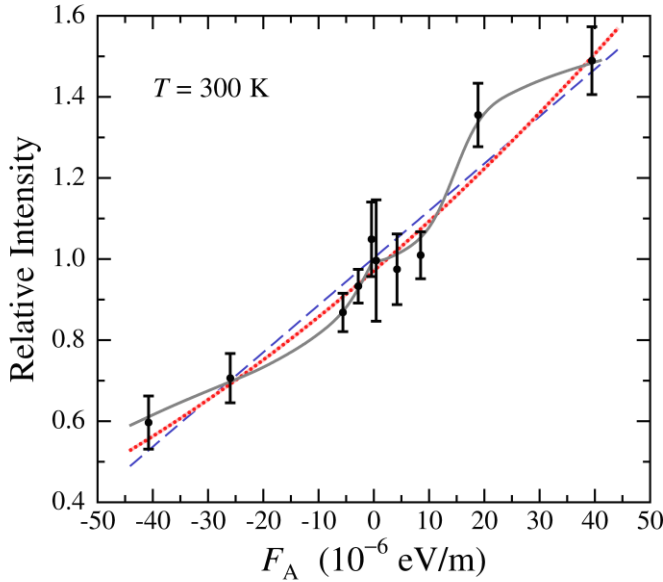


Fig. 5. Relative intensity of slow electrons with various applied forces at room temperature, data symbols and solid trend curves from Ref. [100]. Dashed line shows linear trend; dotted curve is fitted model function of Eq. (15).

where W_0 is the value of W at $F = F_0$ and contains implicit dependence on t . The dotted curve in Fig. 5 shows Eq. (15) with $F_0 = -7.5 \times 10^{-6}$ eV/m, set to the mean value of $-eE$ in Ref. [34], and fitted to the data with $W_0 = 36 \pm 4 \mu\text{V}$ and normalized to $I_r = 0.97 \pm 0.02$ at $F_A = 0$ (reduced $\chi^2 = 0.88$). Uncertainty in F_0 treated as a variable parameter is estimated as $\pm 1.1 \times 10^{-5}$ eV/m, somewhat exceeding the $\pm 6 \times 10^{-6}$ eV/m uncertainty given for eE [34]; F_0 acquires large uncertainty owing to the comparatively weak non-linearity in I_r vs. F_A and scatter in the data.

3.4. Ambient electric field temperature dependence

Data for the variation in the ambient electric field with temperature obtained in the electron free-fall experiments in Refs. [30,34,101] are plotted in Fig. 6 on linear scales. Circle and triangle symbols distinguish the two methods reported for data analysis [34]. The square symbol is the original result in Ref. [30] with error bars reproduced from later work [34,101]. Ambient fields reported for 77 K [$(4 \pm 2) \times 10^{-6}$ V/m] and 300 K [$(7.5 \pm 6) \times 10^{-6}$ V/m] were interpreted as measures of the unshielded electric field E_T [34]. The average $E_T (= 5.75 \times 10^{-6}$ V/m) is assumed for the experimentally determined magnitude, notwithstanding a significant 77% uncertainty [34], which is comparable to $M_{\text{Cu}}g/e = 6.45 \times 10^{-6}$ V/m and the theoretical estimate given in Ref. [27] for Cu mass M_{Cu} .

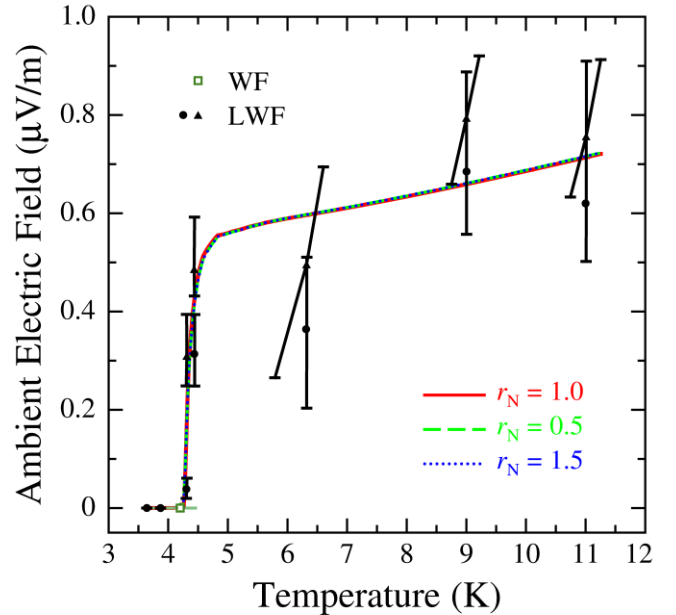


Fig. 6. Ambient electric field inside copper tube vs. temperature. Filled symbols (LWF) denote data from Refs. [34] and [101]; open square symbol (WF) from Ref. [30]. Solid (red), dashed (green), and dotted (blue) curves are obtained with reduced normal-state resistance $r_N = 1.0, 0.5,$ and $1.5,$ respectively.

The theoretical expression for E in Eq. (9) varies with temperature. Temperature dependence is contained in \tilde{S}_s from Eq. (10), T_{BKT} from Eq. (2), and $T_C = \beta n^{1/2}/\zeta$ from Eq. (1), owing to the temperature dependence in charge density n , scaling functionally as

$$n = f_s \theta n_{\text{He}}, \quad (16)$$

where f_s is the fractional number of carriers created per adsorbed ^4He atom and $n_{\text{He}} = 7.9 \times 10^{14} \text{ cm}^{-2}$ is the monolayer capacity [94]. The fractional monolayer coverage θ for inhomogeneous ^4He adsorption is calculated according to Eq. (14), taking values for the binding parameters U_{b0} and σ_b from Section 3.2, helium gas pressure $P = 8 \times 10^{-9}$ Torr from Ref. [34:Erratum], and the constant θ_0 as a fitted parameter. Superconductivity is bounded to $T < T_{\text{CT}}$ at which T_C equals the temperature as defined in terms of the function,

$$T_{\text{CT}} = T_C(T = T_{\text{CT}}). \quad (17)$$

Unknown parameters in the model for ambient electric field E vs. T in Eq. (9) are r_N in Eqs. (4) and (5), f_s in Eq. (16) and θ_0 in Eq. (14). Tube field $E_T = 5.75 \times 10^{-6} \text{ V/m}$ and gravitational field $E_G = -m_e g/e = -5.58 \times 10^{-11} \text{ V/m}$ are treated as known (fixed) quantities. Parameter $b = 1$ in Eq. (10) is assumed for consistency with theory [50]. Given the complex nature of the experimental uncertainties described in Ref. [34], the locations of the symbols and the error bars on linear scales are treated as equally weighted data points. Parameters were obtained from non-linear regression of Eq. (9) to the data subject to the constraint that T_{BKT} at $T = 4.2 \text{ K}$ be in the range 4.2 to 4.4 K, as suggested by the experimental temperature transition and which is found to be satisfied for $r_N \in [0.5, 1.5]$. Results for the fitted parameters and T_{CT} for $r_N = 0.5, 1.0,$ and 1.5 are listed in Table 1 with uncertainties calculated from chi-square χ^2 analysis [90]; there is a parameter correlation given by $f_s \theta_0 \approx 5.1 \times 10^{-4}$. Parameter θ_0 corresponds to a background charge density $f_s \theta_0 n_{\text{He}} = (4 \pm 1) \times 10^{11} \text{ cm}^{-2}$, such as from a submonolayer fraction θ_0 of ^4He accumulated in cryopumped gas [30]. Dependences of E on T are found to have nearly identical forms for $r_N = 0.5, 1.0,$ and 1.5 ($\pm 0.6\%$ variation in χ^2), as shown by the three nearly overlapping model curves in Fig. 6. Figure 7 gives the corresponding temperature dependence in the fractional ^4He coverage θ . Table 2 provides values for the temperature-dependent variables $n, T_C, T_{\text{BKT}}, T_F, \theta, \Lambda_L, \ell, l,$ and $k_F \xi_0$ at $T = 4.2 \text{ K}$ for $r_N = 0.5, 1.0,$ and 1.5 .

Results at the mean $r_N = 1.0$ are $f_s = 0.0598(51)$, $\theta_0 = 0.0086(19)$, and $T_{\text{CT}} = 4.826 \text{ K}$ with root-mean-square

Table 1

Fitted parameters for the fractional charge per ^4He atom f_s , residual ^4He coverage θ_0 , temperature T_{CT} from Eq. (17), and rms deviation between model function and data for the ambient electric field, for reduced normal-state resistance $r_N = 0.5, 1.0,$ and 1.5 .

r_N	f_s	θ_0	T_{CT} (K)	rms deviation ($\mu\text{V/m}$)
0.5	0.0511(48)	0.0101(24)	4.802	0.1533
1.0	0.0598(51)	0.0086(19)	4.826	0.1522
1.5	0.0691(56)	0.0074(16)	4.861	0.1513

deviation from the data of $1.52 \times 10^{-7} \text{ V/m}$, giving $\chi^2 \approx 1.07$. Data and the corresponding model function (red curve) for the absolute value $|E|$ are plotted in Fig. 8 on the left logarithmic scale, which better illustrates the 10^4 dynamic range in the data [30,34,101]. In the model curve, solid denotes the superconducting phase ($T < T_{\text{CT}}$) and dotted denotes the normal phase ($T \geq T_{\text{CT}}$). Variation of T_C and T_{BKT} (right scale) is shown as solid curves for $T < T_{\text{CT}}$; the dotted curves are extended to $T > T_{\text{CT}}$, illustrating the trends.

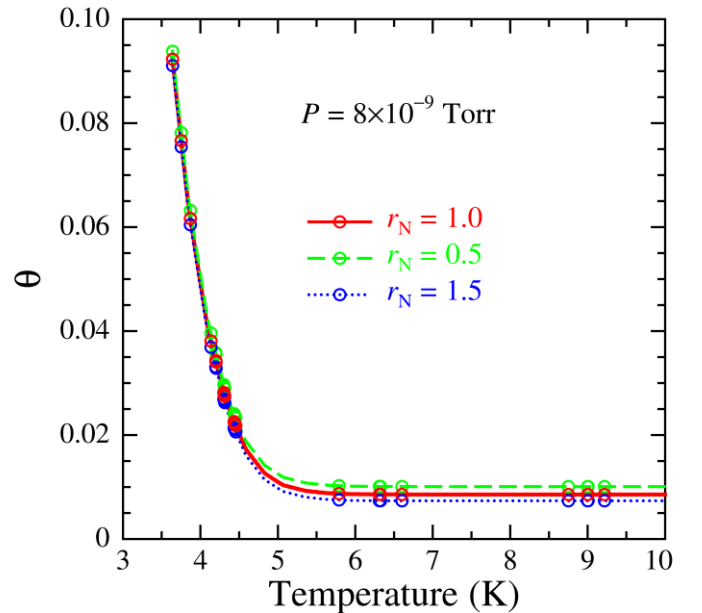


Fig. 7. Temperature variation of ^4He monolayer fraction θ determined from Eq. (14). Solid (red), dashed (green), and dotted (blue) curves are obtained with reduced normal-state resistance $r_N = 1.0, 0.5,$ and $1.5,$ respectively. Symbols are at the temperatures in the data.

Table 2

Parameters of the superconducting layer at $T = 4.2$ K for reduced normal-state resistance $r_N = 0.5, 1.0,$ and 1.5 : carrier density n , transition temperature T_C , BKT temperature T_{BKT} , Fermi temperature T_F , adsorbed ^4He fraction θ , London penetration depth Λ_L , carrier spacing ℓ , mean free path l , and product of Fermi wavevector k_F and coherence distance ξ_0 ; parameter ξ_0 is constant with temperature.

r_N	n (10^{12} cm^{-2})	T_C (K)	T_{BKT} (K)	T_F (K)	θ	Λ_L (cm)	ℓ (Å)	l (Å)	$k_F \xi_0$	ξ_0 (Å)
0.5	1.44	7.49	4.46	58.1	0.0357	0.270	83.2	266	1.97	65.6
1.0	1.61	7.92	4.40	65.0	0.0342	0.241	78.7	126	2.09	65.6
1.5	1.80	8.37	4.33	72.6	0.0330	0.216	74.5	79	2.21	65.6

At 4.2 K, the ratio $n/m^* = 2.3 \times 10^{12} \text{ cm}^{-2} m_e^{-1}$ is $\sim 84\%$ of the value deduced from the effect of ^4He on the work function, yielding $E_F = 5.6$ meV. Non-universal τ_C in Eq. (10) is temperature dependent and of magnitude 0.8 at 4.2 K. Reported results for τ_C give 0.02 to 0.24 for granular films [69,85], 0.21 to 0.47 for amorphous films [85], and 0.3 to greater than 0.9 for gate-charged twisted bilayer graphene [39].

Since $k_F a \approx 0.014$, for (room temperature) lattice constant $a = 4.27 \text{ Å}$ for Cu_2O and $k_F = (3.19 \pm 0.02) \times 10^6$

cm^{-1} at $T = 4.2$ K, some of the surface roughness from nanoscale faceting, surface steps, and incommensurate epitaxy tends to be smoothed out. The characteristic length scale l for carrier scattering corresponds to a range of 20 to 60 lattice parameters.

This model obviously presumes that a sub-monolayer of adsorbed ^4He is required for the superconducting shielding, yielding $E = E_G$ at $T \leq 4.2$ K. The abrupt change in temperature dependence for $T > 4.2$ K arises from thermal desorption of ^4He in combination with fluctuation superconductivity and the transition to the normal state. The form of observed transition in the ambient field is influenced mostly by data at $T \sim 4.2 - 4.4$ K and is for the most part described by the model function curves in Figs. 6 and 8.

4. Discussion

The functional dependence of T_C on carrier density, varying as $n^{1/2}$ in Eq. (1), derives from a model of two-dimensional superconductivity mediated by interlayer Coulomb coupling [21,102]. As shown from a pairing ansatz variational model, the zero-temperature gap Δ also varies as $n^{1/2}$, which is attributed to the constant density of normal electronic states in two-dimensions [1]. These results, obtained from different approaches, evidently constitute equivalent theoretical findings and stand in contrast to three dimensions, where dependence on n appears in an exponent [1].

Equation (1) determines $k_B T_C$ as the product of a strong interlayer Coulomb potential e^2/ζ and a small interaction factor Λ/ℓ , which evaluate to 7.20 eV and $(9.8 \pm 0.5) \times 10^{-5}$, respectively, for $\zeta = 2.0 \text{ Å}$ and $\ell = 79 \pm 4 \text{ Å}$ (Table 2). These factors derive from the concept of superconductivity propagating via quantum fluctuations within the virtual photon field formed between the two charge reservoirs via a Compton-effective scattering of quasiparticles confined to their respective reservoirs (see,

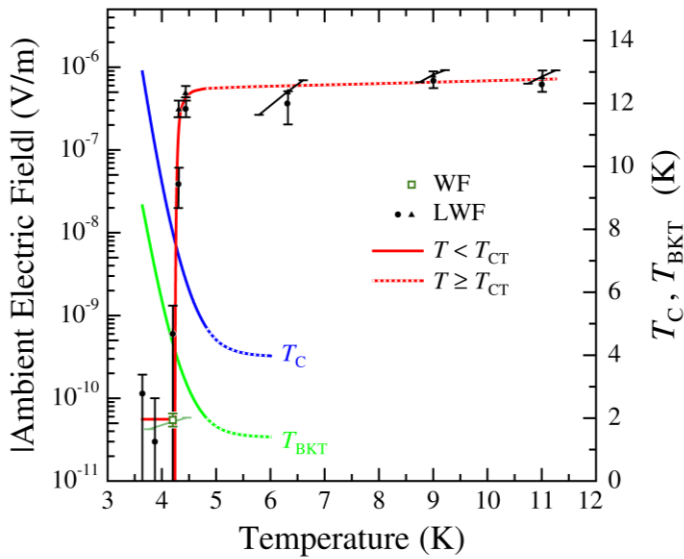


Fig. 8. Absolute value of the ambient electric field inside copper tube vs. temperature. Filled symbols (LWF) denote data from Refs. [34] and [100]; open square symbol (WF) and vertical error bars from Ref. [30] (slanted error bars from Ref. [34]). The red curve shows the absolute value of ambient field calculated from Eqs. 9 and 10, left scale, with temperature dependences in T_C (blue curve) and T_{BKT} (green curve), right hand scale; superconducting region is denoted by solid curves, normal region by dotted curves.

e.g., Ref. [102]), with optimal superconductivity occurring upon charge equilibration between the interacting quasiparticles of the two reservoirs. Asymmetry between (+) and (-) charges is established for Cu/CuO₂ by differing dynamics of mobile Cu₂O (+) charges and quasi-localized (-) at Cu sites, in addition to the interlayer separation. Thus, pairing occurs between two (+) Fermion charges in the Cu₂O layer mediated via exchange of virtual photons with a (-) charge in Cu [21]. While uncertainty exists regarding how the (-) charges are distributed in the Cu, a plausible scenario is a quasi-static distribution of charge reflecting the pattern of adsorbed He atoms. Hence, the (-) charges are quasi-localized in Cu by variable interface bonding potentials, whereas the (+) charges in Cu₂O occupy a high mobility interface band. Note also that the mechanism driving the pairing interaction is, by its nature, instantaneous, as in the case treated in Ref. [91] concerning low carrier density superconductors. Unfortunately, there are, at present, no first-principles methods (e.g., based on density functional perturbation theory [103]), since the energies $\sim e^2/\zeta$ of the two virtual photons greatly exceed E_F , even with differences in pair momenta small compared to k_F .

4.1. Bosonic effects

Proximity of the 2D superconductivity to a bosonic pairing phase is determined below, following from parameters determined for Cu/Cu₂O with ⁴He adsorption. It may be noted that participation of a fraction of the paired charges in a Bose condensate is sufficient to produce the shielding of ambient electric fields observed in the electron free-fall experiments. For the condensed ideal 2D Bose gas treated in Ref. [12], a theoretical estimate for the shielding factor is $S \approx k_B T / (4\pi e^2 \zeta n N_0)$, where N_0 is the ground state occupation number and ζ is the assumed thickness. An experimental value for the shielding factor at $T = 4.2$ K may be approximated as the ratio of the experimental resolution $0.09 mg/e$ to the unshielded E_T , giving $S \sim 8 \times 10^{-6}$ as an upper limit. This value in the theoretical expression suggests $N_0 \approx 8 \times 10^3$ as the lower limit. As estimated in Section 2.2, a number $N_v \approx 10^8$ vortices perforate the 2D superconductor, with each core containing about $(n/2)\pi\zeta^2 \approx 4.6$ pairs at 4.2 K. Conjecturing that vortex cores supply a reservoir of non-superconducting bosonic pairs (assuming $\Delta \rightarrow 0$ at the vortex core), the observed S is realized with a fraction $\sim 10^{-4}$ of core pairs forming a coexisting Bose condensate.

The length ζ in the Coulomb interaction potential is short relative to the Cooper pair size as well as the inter-particle separation, because the ratio $\zeta/\xi_0 = (\pi/2)^{1/2} \beta k_B m^* / \hbar^2$ acquires the fixed value of 0.0305 in the present case and $k_F \zeta = 0.064 \pm 0.004$ is obtained at $T = 4.2$ K from modeling the ambient electric field data.

Additionally, the superconductive pairing occurs at low carrier density, $k_F \xi_0 = 2.1 \pm 0.1$, which lies near the crossover ($k_F \xi_0 \sim 1$) from superconductivity to Bose-Einstein condensation [1,91,104,105]. Considering that pairing interactions have a relatively short range, useful guidance is provided from calculations of the crossover in 2D that employ short-range or contact interactions and find smooth evolution in the equation of state, pair wavefunction shape, and phase diagram as functions of the interaction parameter $k_F a_{2D}$ (a_{2D} defines the interaction length) [2,9]. Values of T_{BKT}/T_F from Table 2 in combination with the phase diagram for T_{BKT}/T_F vs. $\ln(k_F a_{2D})$ calculated for contact attraction in a 2D Fermi gas [9] lead to the prediction $a_{2D} = 141 \pm 18$ Å, a functional form of T_{BKT} vs. T_F analogous to Eq. (3), and calculated curves for the ambient electric field nearly replicating the results for $r_N \approx 1$ (rms deviation of 0.1518 $\mu V/m$ with respect to the data).

Equation (3) may be expressed in terms of the Fermi wavevector as,

$$T_{BKT} / T_F = f_C [8\epsilon_C (1 + 0.75 r_N k_F \xi_0 / 4)]^{-1}, \quad (18)$$

and using Eq. (1) to evaluate $f_C = f[(\pi/2)^{1/2} \hbar^2 k_F \zeta t_{BKT} / \beta k_B m^*]$

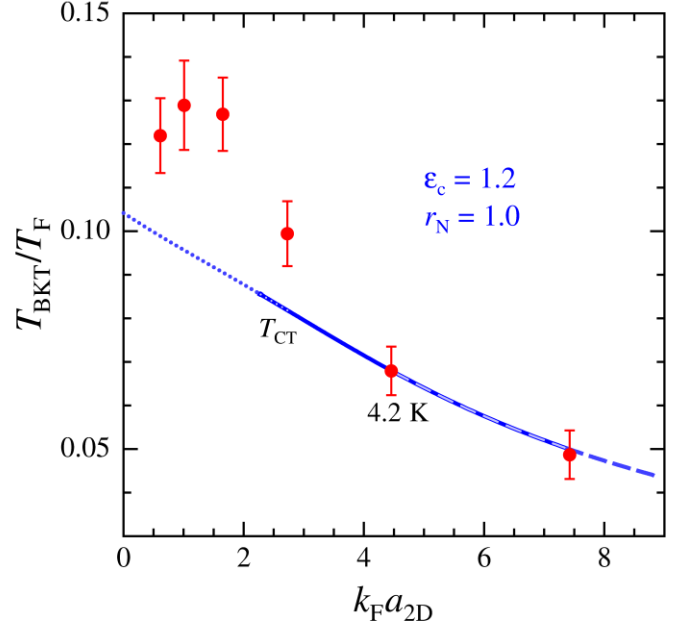


Fig. 9. Ratio T_{BKT} / T_F vs. interaction parameter $k_F a_{2D}$ from Eq. (18) for parameters $\epsilon_C = 1.2$ and $r_N = 1.0$, shown as the solid curve in the temperature range of the ambient field data, dotted overlay for $T > T_{CT}$ and dashed overlay for $T < 4.2$ K; extensions of the curves outside the data range is shown as dotted (left) and dashed (right). Numerical calculations from Ref. [9] are shown as the symbols with error bars.

with the definition $t_{\text{BKT}} \equiv T_{\text{BKT}}/T_{\text{F}}$. For a fixed r_{N} , as in Section 2.1, this form gives $T_{\text{BKT}}/T_{\text{F}} = 1/8\varepsilon_{\text{C}}$ in the dilute limit $k_{\text{F}} \rightarrow 0$. The dependence of the ratio for $\varepsilon_{\text{C}} = 1.2$ and $r_{\text{N}} = 1.0$ on $k_{\text{F}}a_{2\text{D}}$ is plotted in Fig. 9. The solid underlay curve corresponds to the temperature range 3.64 to 11.25 K in the ambient electric field data, for which $k_{\text{F}}a_{2\text{D}} \in (2.26, 7.38)$. The region $T < 4.2$ K ($k_{\text{F}}a_{2\text{D}} > 7.38$) is shown with a dashed overlay and the region $T > T_{\text{CT}}$ ($k_{\text{F}}a_{2\text{D}} < 2.26$) with a dotted overlay. Two broken curves extending beyond the range of the data are shown as dotted for $k_{\text{F}}a_{2\text{D}} \rightarrow (\ll 1)$ and as dashed for $k_{\text{F}}a_{2\text{D}} \rightarrow (\gg 1)$. For comparison, the filled symbols (error bars) show the continuum scaling results from numerical calculations (Fig. 1 in Ref. [9]). The good agreement between the numerical points and the curve in the region corresponding to T up to about 4.2 K underlies the equivalent results in modeling the temperature transition in the ambient electric field discussed in Section 3. It also provides validation of the function of Eq. (1), which predicts that T_{C} scales with k_{F} . Extension of the range in the function for $T_{\text{BKT}}/T_{\text{F}}$ vs. $k_{\text{F}}a_{2\text{D}}$ according Eq. (18) shows a linear approach to the upper bound of $1/8\varepsilon_{\text{C}}$ at $k_{\text{F}}a_{2\text{D}} \rightarrow 0$, whereas the numerical results reach an upper bound of $1/8 \pm 0.008$ for $k_{\text{F}}a_{2\text{D}} \sim 1$ and appear to find $\varepsilon_{\text{C}} \rightarrow 1 \pm 0.06$ in this regime.

The pair binding energy, defined as $E_{\text{b}} = 4 \exp(-2\gamma_{\text{E}})\hbar^2/m^*a_{2\text{D}}^2$ (where $\gamma_{\text{E}} \simeq 0.5771$ is Euler's constant) [2], yields $E_{\text{b}} = 0.7 \pm 0.2$ meV. This result ($E_{\text{b}}/k_{\text{B}} = 8 \pm 2$ K) predicts an appreciable density of bound pairs at $T = 4.2$ K, where $\ln(k_{\text{F}}a_{2\text{D}}) = 1.5 \pm 0.2$, which could allow a minority BEC-like component to coexist and be sustained by the majority superconducting phase for $T < T_{\text{BKT}}$. In a mean field model, the binding energy is obtained as $E_{\text{b}} = \Delta_0^2/2E_{\text{F}}$ [1]. Combining Eq. (1), $\Delta_0 = \gamma k_{\text{B}}T_{\text{C}}$, and $E_{\text{F}} = \pi\hbar^2n/m^*$, one obtains an expression $E_{\text{b}} = [3.97(3)] (\gamma^2\alpha^2/\pi) (m^*/m_{\text{e}}) \hbar^2/2m_{\text{e}}\zeta^2$ which is nominally independent of carrier density, where α is the fine structure constant. Consequently, $a_{2\text{D}}$ is predicted to be independent of n . Evaluation for $\gamma = 2.5$, $m^* = 0.69 m_{\text{e}}$, and $\zeta = 2.0$ Å (and $\hbar^2/2m_{\text{e}}\zeta^2 = 0.95$ eV) produces a value smaller than above; $E_{\text{b}} = 0.26$ meV (or $E_{\text{b}}/k_{\text{B}} = 3.0$ K).

4.2. Weak equivalence principle test

The original gravitational instrumentation was deemed adaptable for measuring the gravitational force on the positron [31,100] and potentially testing the weak equivalence principle (WEP) of general relativity theory. Note that an argument was posed that Schiff-Barnhill effects render the vertical geometry insensitive for testing the WEP for electrons [106]. Alternative geometries with relativistic or near-relativistic horizontal velocities and non-relativistic vertical velocities have been suggested for improved accuracy in measuring the ratio of inertial and gravitational masses by reducing perturbations by the DMRT and patch fields [107-109]. Near weightless

environments are clearly advantageous [106], and a test conducted in Earth's orbit found equivalence to a precision on order 10^{-15} [110]. Recent experiments using antihydrogen, which has the advantage of being charge neutral, find downward gravitational acceleration consistent with the WEP [111]; the magnitude for antihydrogen, given as $0.75g$ and uncertainties summing to $0.29g$, is evidently less certain than $(0.98 \pm 0.09)g$ originally determined for the electron [30,31].

4.3. Shielding ambient electric fields

In the proposed model, the superconducting layer on the copper tube yields a shielding factor $S \ll S_{\text{N}}$ at 4.2 K, where the charges induced by adsorbed ^4He yield T_{BKT} of at least 4.3 K. For $T > 4.2$ K, the value of T_{BKT} falls below 4.2 K, owing to desorption of ^4He and diminished charge density, such that the onset of superconducting phase fluctuations causes a rapid increase of S towards S_{N} . As T_{C} drops with increasing temperature, the superconductor undergoes a transition to the normal state at $T_{\text{CT}} = T_{\text{C}} = 4.83 \pm 0.03$ K (denoted by the dotted/solid boundary in Fig. 8). Effects of phase fluctuations and ^4He desorption therefore account for most of abrupt increase in the ambient electric field observed in the heated tube experiment (Figs. 6 and 8) [34,100]. Ambient electric field data for $6 \text{ K} \lesssim T \lesssim 11 \text{ K}$ indicate $S = S_{\text{N}}$ for an electron layer in the normal state, possibly caused by residual ^4He commingled with other adsorbed ambient gas species. Surface charges as considered in the earlier models [12,43] remain a possibility. Work function data [87,35] confirm the plausibility of superconducting and non-superconducting electronic charges coexisting on the surface of native-oxidized copper and the correlation of induced charge with adsorbed ^4He .

5. Conclusion

Based on previous work on interlayer Coulomb mediation [21,38,102], a model is presented for interfacial superconductivity, arising in a semiconductor-on-metal structure from Coulomb interactions between interface charges in the semiconductor and corresponding screening charges in the metal surface, and considered for the case Cu/Cu₂O. The intrinsic superconducting transition temperature T_{C} for such an interaction scales with the areal density of superconducting charges as $n^{1/2}$ and inversely with the separation ζ between the two charge layers. Application of this model is offered as an explanation for the shielding of lattice compression and patch electric fields from the copper drift tube observed in the gravitational electron free fall experiments at $T \approx 4.2$ K [30] and the temperature dependence observed in the heated tube experiment [34]. It is also shown that electron- ^4He scattering is much weaker than previously

supposed [34,36] and supports the validity of ambient field data for $T > 4.2$ K as originally reported [34].

Superconducting charges in Cu_2O at the Cu interface and screening charges in the Cu are induced by an inhomogeneous sub-monolayer of adsorbed ^4He . By modeling temperature-dependent inhomogeneous adsorption of sub-monolayer ^4He , n and transition temperatures T_C and T_{BKT} become diminishing functions of increasing T , owing to ^4He desorption, and constraining superconductivity to the region $T < 4.83 \pm 0.03$ K. For $\theta \approx 0.034$ monolayers of ^4He coverage at $T = 4.2$ K, $n = (1.6 \pm 0.2) \times 10^{12} \text{ cm}^{-2}$ and theoretically projected $T_C = 7.9 \pm 0.4$ K are calculated for $\zeta = 2.0 \text{ \AA}$, as estimated from interface structure calculations. Finally, it is important to note that $T_C \propto n^{1/2}$ is equivalent to energy gap $\Delta \propto n^{1/2}$ derived for low carrier density superconductors in two dimensions [1].

CRedit authorship contribution statement

Dale R. Harshman: Conceptualization, Data curation, Formal analysis, Investigation, Methodology, Project administration, Resources, Software, Supervision, Validation, Visualization, Writing – original draft, Writing – review & editing. **Anthony T. Fiory:** Conceptualization, Data curation, Formal analysis, Investigation, Methodology, Project administration, Resources, Software, Supervision, Validation, Visualization, Writing – original draft, Writing – review & editing.

Declaration of Competing Interest

The authors declare that they have no known competing financial interests or personal relationships that could have appeared to influence the work reported in this paper.

Data availability

Data shown in the figures are available in the cited references.

Acknowledgements

The authors are grateful for support from the University of Notre Dame, and greatly appreciate communications from F. W. Witteborn and J. M. Lockhart on their readings of an early version of the manuscript.

References

- [1] M. Randeria, J.-M. Duan, L.-Y. Shieh, Superconductivity in a two-dimensional Fermi gas: evolution from Cooper pairing to Bose condensation, *Phys. Rev. B* 41 (1990) 327.
- [2] G. Bertaina, S. Giorgini, BCS-BEC crossover in a two-dimensional Fermi gas, *Phys. Rev. Lett.* 106 (2011) 110403.

- [3] S. Gariglio, M. Gabay, J. Mannhart, J.-M. Triscone, Interface superconductivity, *Physica C: Supercond. Applic.* 514 (2015) 189.
- [4] T. Hazra, N. Verma, M. Randeria, Bounds on the superconducting transition temperature: applications to twisted bilayer graphene and cold atoms, *Phys. Rev. X* 9 (2019) 031049.
- [5] C. Yang, Y. Liu, Y. Wang, L. Feng, Q. He, J. Sun, Y. Tang, C. Wu, J. Xiong, W. Zhang, X. Lin, H. Yao, H. Liu, G. Fernandes, J. Xu, J.M. Valles Jr., J. Wang, Y. Li, Intermediate bosonic metallic state in the superconductor-insulator transition, *Science* 366 (2019) 1505.
- [6] Y. Nakagawa, Y. Kasahara, T. Nomoto, R. Arita, T. Nojima, Y. Iwasa, Gate-controlled BCS-BEC crossover in a two-dimensional superconductor, *Science* 372 (2021) 190.
- [7] D. Qui, C. Gong, S.-S. Wang, M. Zhang, C. Yang, X. Wang, J. Xiong, Recent advances in 2D superconductors, *Adv. Mater.* 33 (2021) 2006124.
- [8] M. Randeria, Limits on superconductivity in flatland, *Science* 372 (2021) 132.
- [9] Y.-Y. He, H. Shi, S. Zhang, Precision many-body study of the Berezinskii-Kosterlitz-Thouless transition and temperature-dependent properties in the two-dimensional Fermi gas, *Phys. Rev. Lett.* 129 (2022) 076403.
- [10] Z. Wang, Y. Liu, C. Ji, J. Wang, Quantum phase transitions in two-dimensional superconductors: a review on recent experimental progress, *Rep. Prog. Phys.* 87 (2024) 014502.
- [11] H. Ji, Y. Liu, C. Ji, J. Wang, Two-dimensional and interface superconductivity in crystalline systems, *Acc. Mater. Res.* 5 (2024) 1146.
- [12] R.S. Hanni, J.M.J. Madey, Shielding by an electron surface layer, *Phys. Rev. B* 17 (1978) 1976.
- [13] V.L. Ginzburg, D.A. Kirzhnits, On the superconductivity of electrons at the surface levels, *Zh. Eksp. Teor. Fiz.* 46 (1964) 397 [*Sov. Phys. JETP* 19 (1964) 269].
- [14] V.L. Ginzburg, The problem of high-temperature superconductivity II, *Usp. Fiz. Nauk* 101 (1970) 185 [*Sov. Phys. Usp.* 13 (1970) 335].
- [15] D. Allender, J. Bray, J. Bardeen, Model for an exciton mechanism of superconductivity, *Phys. Rev. B* 7 (1973) 1020.
- [16] J.C. Inkson, Schottky barriers and plasmons, *J. Vac. Sci. Technol.* 11 (1974) 943.
- [17] W.A. Little, Generalization of BCS superconductivity to non-phonon mediated interactions: the excitonic interaction, in: S. Maekawa, M. Sato (Eds.), *Physics of High-Temperature Superconductors*, Springer Series in Solid-State Sciences, vol. 106, Springer, Berlin, Heidelberg, 1992, p. 113.
- [18] R. Arita, Y. Tanida, K. Kuroki, H. Aoki, Image-potential band-gap narrowing at a metal/semiconductor interface, *Phys. Rev. B* 64 (2001) 245112.
- [19] M. Kiguchi, K. Saiki, Metal-induced gap states at insulator/metal interfaces, *e-J. Surf. Sci. Nanotech.* 2 (2004) 191.

- [20] V. Körting, Q. Yuan, P.J. Hirschfeld, T. Kopp, J. Mannhart, Interface-mediated pairing in field effect devices, *Phys. Rev. B* 71 (2005) 104510.
- [21] D.R. Harshman, A.T. Fiory, J.D. Dow, Theory of high- T_C superconductivity: transition temperature, *J. Phys.: Condens. Matter* 23 (2011) 295701. Corrigendum: *J. Phys.: Condens. Matter* 23 (2011) 349501.
- [22] S. K. Chawla, B.I. Rickett, N. Sankarraman, J.H. Payer, An X-ray photoelectron spectroscopic investigation of the air-formed film on copper, *Corrosion Sci.* 33 (1992) 1617.
- [23] T.L. Barr, An ESCA study of the termination of the passivation of elemental metals, *J. Phys. Chem.* 82 (1978) 1801.
- [24] B. Devine, T.-R. Shan, Y.-T. Cheng, A.J.H. McGaughey, M. Lee, S.R. Phillpot, S.B. Sinnott, Atomistic simulations of copper oxidation and Cu/Cu₂O interfaces using charge-optimized many-body potentials, *Phys. Rev. B* 84 (2011) 125308. Erratum: *Phys. Rev. B* 85 (2012) 199904.
- [25] C. Herring, M.H. Nichols, Thermionic emission, *Rev. Mod. Phys.* 21 (1949) 185.
- [26] L.I. Schiff, Gravitation-induced electric field near a metal. II, *Phys. Rev. B* 1 (1970) 4649.
- [27] A.J. Dessler, F.C. Michel, H.E. Rorschach, G.T. Trammell, Gravitationally induced electric fields in conductors, *Phys. Rev.* 168 (1968) 737.
- [28] C. Herring, Gravitationally induced electric field near a conductor, and its relation to the surface-stress concept, *Phys. Rev.* 171 (1968) 1361.
- [29] T.J. Rieger, Gravitationally induced electric fields in metals, *Phys. Rev. B* 2 (1970) 825.
- [30] F.C. Witteborn, W.M. Fairbank, Experimental comparison of the gravitational force on freely falling electrons and metallic electrons, *Phys. Rev. Lett.* 19 (1967) 1049.
- [31] F.C. Witteborn, W.M. Fairbank, Experiments to determine the force of gravity on single electrons and positrons, *Nature* 220 (1968) 436.
- [32] G.S. LaRue, W.M. Fairbank, A.F. Hebard, Evidence for the existence of fractional charge on matter, *Phys. Rev. Lett.* 38 (1977) 1011.
- [33] A.F. Hebard, A superconducting suspension with variable restoring force and low damping, *Rev. Sci. Instrum.* 44 (1973) 425.
- [34] J.M. Lockhart, F.C. Witteborn, W.M. Fairbank, Evidence for a temperature-dependent surface shielding effect in Cu, *Phys. Rev. Lett.* 38 (1977) 1220. Erratum: *Phys. Rev. Lett.* 67 (1991) 283.
- [35] A.Th.A.M. de Waele, R. de Bruyn Ouboter, P.B. Pipes, Thermo-electrostatic effects in superconductors, *Physica* 65 (1973) 587.
- [36] T.W. Darling, F. Rossi, G.I. Opat, G.F. Moorhead, The fall of charged particles under gravity: a study of experimental problems, *Rev. Mod. Phys.* 64 (1992) 237.
- [37] J.C. Inkson, The electrostatic image potential in metal semiconductor junctions, *J. Phys. C: Solid State Phys.* 4 (1971) 591.
- [38] D.R. Harshman, A.T. Fiory, High- T_C superconductivity in ultra-thin crystals: implications for microscopic theory, *Emerg. Mater. Res.* 1 (2012) 4.
- [39] D.R. Harshman, A.T. Fiory, High- T_C superconductivity originating from interlayer Coulomb coupling in gate-charged twisted bilayer graphene Moiré superlattices, *J. Supercond. Nov. Magn.* 33 (2020) 367.
- [40] L.I. Schiff, M.V. Barnhill, Gravitation-induced electric field near a metal, *Phys. Rev.* 151 (1966) 1067.
- [41] F.C. Witteborn, W.M. Fairbank, Apparatus for measuring the force of gravity on freely falling electrons, *Rev. Sci. Instrum.* 48 (1977) 1.
- [42] A.R. Hutson, Electrons of the vacuum surface of copper oxide and the screening of patch fields, *Phys. Rev. B* 17 (1978) 1934.
- [43] J. Bardeen, Comments on shielding by surface states, in: J.D. Fairbank, B.S. Deaver Jr., C.W.F. Everitt, P.R. Michelson (Eds.), *Near Zero: New Frontiers of Physics*, Freeman, New York, 1988, p. 874.
- [44] Y.H. Lin, J. Nelson, A.M. Goldman, Superconductivity of very thin films: the superconductor-insulator transition, *Physica C Supercond. Applic.* 514 (2015) 130.
- [45] C.A. Waters, H.A. Fairbank, J.M. Lockhart, K.W. Rigby, Low temperature transition in the microwave surface impedance of copper, in: J.D. Fairbank, B.S. Deaver Jr., C.W.F. Everitt, P.R. Michelson (Eds.), *Near Zero: New Frontiers of Physics*, Freeman, New York, 1988, p. 861.
- [46] J.W. Hodby, T.E. Jenkins, C. Schwab, H. Tamura, D. Trivich, Cyclotron resonance of electrons and of holes in cuprous oxide, Cu₂O, *J. Phys. C: Solid State Phys.* 9 (1976) 1429.
- [47] V.L. Berezinskiĭ, Destruction of long-range order in one-dimensional and two-dimensional systems having a continuous symmetry group I. Classical systems, *Zh. Eksp. Teor. Fiz.* 59 (1970) 907 [*Sov. Phys. JETP* 32 (1971) 493].
- [48] V.L. Berezinskiĭ, Destruction of long-range order in one-dimensional and two-dimensional systems possessing a continuous symmetry group II. Quantum systems, *Zh. Eksp. Teor. Fiz.* 61 (1971) 1144 [*Sov. Phys. JETP* 34 (1972) 610].
- [49] J.M. Kosterlitz, D.J. Thouless, Ordering, metastability and phase transitions in two-dimensional systems, *J. Phys. C: Solid State Phys.* 6 (1973) 1181.
- [50] B.I. Halperin, D.R. Nelson, Resistive transition in superconducting films, *J. Low Temp. Phys.* 36 (1979) 599.
- [51] J.B. Condon, *Surface Area and Porosity Determinations by Physisorption: Measurement, Classical Theories and Quantum Theory* 2nd Edn., Elsevier, Amsterdam, 2019
- [52] N.P. Danilova, A.I. Shal'nikov, The adsorption of helium on a copper surface at 4.2 °K, *Cryogenics* 8 (1968) 322.
- [53] J.M. Lockhart, RF impedance measurements on granular superconducting and normal thin films, *Physica* 107B (1981) 487.

- [54] J.C. Inkson, Many-body effect at metal-semiconductor junctions. II. The self energy and band structure distortion, *J. Phys. C: Solid State Phys.* 6 (1973) 1350.
- [55] W.H. Brattain, The copper oxide rectifier, *Rev. Mod. Phys.* 23 (1951) 203.
- [56] L.J. Brillson, The structure and properties of metal-semiconductor interfaces, *Surf. Sci. Rep.* 2 (1982) 123.
- [57] D.A. Muller, D.A. Shashkov, R. Benedek, L.H. Yang, J. Silcox, D.N. Seidman, Atomic scale observations of metal-induced gap states at {222} MgO/Cu interfaces, *Phys. Rev. Lett.* 80 (1998) 4741.
- [58] O.Yu. Kolesnychenko, O.I. Shklyarevskii, H. van Kempen, Anomalous increase of the work function in metals due to adsorbed helium, *Physica B* 284-288 (2000) 1257.
- [59] E. Zaremba, W. Kohn, Theory of helium adsorption on simple and noble-metal surfaces, *Phys. Rev. B* 15 (1977) 1769.
- [60] N.D. Lang, J.K. Nørskov, Interaction of helium with a metal surface, *Phys. Rev. B* 27 (1983) 4612.
- [61] G. Ihm, M.W. Cole, Calculation of physisorption potentials in the electron gas approximation, *Langmuir* 5 (1989) 550.
- [62] N.D. Lang, W. Kohn, Theory of metal surfaces: work function, *Phys. Rev. B* 3 (1971) 1215.
- [63] V. Petit, M. Taborelli, H. Neupert, P. Chiggiato, M. Belhaj, Role of the different chemical components in the conditioning process of air exposed copper surfaces, *Phys. Rev. Accel. Beams* 22 (2019) 083101.
- [64] S.N. Sami, L. Diaz, M. Sanati, R.P. Joshi, Simulations of field emission from copper electrodes with inclusion of oxygen surface layer and work function changes based on first-principles calculations, *J. Appl. Phys.* 128 (2020) 223302.
- [65] A. Hallil, J.-M. Raulot, M. Cherkaoui, Atomistic simulations of Cu₂O bulk and Cu/Cu₂O interface properties by using a new interatomic potential, *Comp. Mater. Sci.* 81 (2014) 366.
- [66] F. Chiter, D. Costa, V. Maurice, P. Marcus, DFT-based Cu(111)||Cu₂O(111) model for copper metal covered by ultrathin copper oxide: structure, electronic properties, and reactivity, *J. Phys. Chem. C* 124 (2020) 17048.
- [67] N.D. Lang, W. Kohn, Theory of metal surfaces: induced surface charge and image potential, *Phys. Rev.* 7 (1973) 3541.
- [68] W.L. Ginzburg, Concerning surface superconductivity, *Zh. Eksp. Teor. Fiz.* 47 (1964) 2318 [*Sov. Phys. JETP* 20 (1965) 1549].
- [69] A.M. Kadin, K. Epstein, A.M. Goldman, Renormalization and the Kosterlitz-Thouless transition in a two-dimensional superconductor, *Phys. Rev. B* 27 (1983) 6691.
- [70] M. Tinkham, *Introduction to Superconductivity*, McGraw Hill, New York, 1996 second ed.
- [71] D.R. Harshman, W.J. Kossler, X. Wan, A.T. Fiory, A.J. Greer, D.R. Noakes, C.E. Stronach, E. Koster, J.D. Dow, Nodeless pairing-state in single-crystal YBa₂Cu₃O₇, *Phys. Rev. B* 69 (2004) 174505.
- [72] D.R. Nelson, J.M. Kosterlitz, Universal jump in the superfluid density of two-dimensional superfluids, *Phys. Rev. Lett.* 39 (1977) 1201.
- [73] M.R. Beasley, J.E. Mooij, T.P. Orlando, Possibility of vortex-antivortex pair dissociation in two-dimensional superconductors, *Phys. Rev. Lett.* 42 (1979) 1165.
- [74] B.G. Orr, H.M. Jaeger, A.M. Goldman, C.G. Kuper, Global phase coherence in two-dimensional granular superconductors, *Phys. Rev. Lett.* 56 (1986) 378. Erratum: *Phys. Rev. Lett.* 56 (1986) 996.
- [75] S. Chakravarty, G.-L. Ingold, S. Kivelson, A. Luther, Onset of global phase coherence in Josephson-junction arrays: a dissipative phase transition, *Phys. Rev. Lett.* 56 (1986) 2303.
- [76] H.M. Jaeger, D.B. Haviland, B.G. Orr, A.M. Goldman, Onset of superconductivity in ultrathin granular metal films, *Phys. Rev. B* 40 (1989) 182.
- [77] V. Ambegaokar, A. Baratoff, Tunneling between superconductors, *Phys. Rev. Lett.* 10 (1963) 486. Erratum *Phys. Rev. Lett.* 11 (1963) 104.
- [78] C.J. Lobb, D.W. Abraham, M. Tinkham, Theoretical interpretation of resistive transition data from arrays of superconducting weak links, *Phys. Rev. B* 27 (1983) 150.
- [79] P.G. de Gennes, Boundary effects in superconductors, *Rev. Mod. Phys.* 36 (1964) 225.
- [80] R.S. Newrock, C.J. Lobb, U. Geigenmüller, M. Octavio, The two-dimensional physics of Josephson junction arrays, *Sol. State Phys.* 54 (2000) 263.
- [81] P. Lipavský, J. Koláček, K. Morawetz, E.H. Brandt, Electrostatic potential in a superconductor, *Phys. Rev. B* 65 (2002) 144511.
- [82] J. Koláček, P. Lipavský, Thermopower in superconductors: temperature dependence of magnetic flux in a bimetallic loop, *Phys. Rev. B* 71 (2005) 092503.
- [83] A.T. Fiory, B. Serin, Observation of a “Peltier” effect in a type-II superconductor, *Phys. Rev. Lett.* 16 (1966) 308.
- [84] P.R. Solomon, F.A. Otter Jr., Thermomagnetic effects in superconductors, *Phys. Rev.* 164 (1967) 608.
- [85] A.T. Fiory, A.F. Hebard, W.I. Glaberson, Superconducting phase transitions in indium/indium-oxide thin-film composites, *Phys. Rev. B* 28 (1983) 5075.
- [86] J. Bardeen, M.J. Stephen, Theory of the motion of vortices in superconductors, *Phys. Rev. B* 140 (1965) A1197.
- [87] J.U. Free, C.D. Dermer, P.B. Pipes, Temperature derivative of the electronic work function of copper at low temperatures, *Phys. Rev. B* 19 (1979) 631.
- [88] D.H. Darling, P.B. Pipes, The effect of the superconducting transition on the electronic work function of niobium, *Physica* 85B (1977) 277.
- [89] J.U. Free, C.D. Dermer, P.B. Pipes, Effect of helium gas on the contact potential of copper between 2 and 20 K, *Bull. Am. Phys. Soc.* 23 (1978) 565.

- [90] P.B. Bevington, *Data Reduction and Error Analysis for the Physical Sciences*, McGraw-Hill, New York, 1969.
- [91] D. van der Marel, Anomalous behaviour of the chemical potential in superconductors with a low density of carriers, *Physica C* 165 (1990) 35.
- [92] M. Randeria, E. Taylor, Crossover from Bardeen-Cooper-Schrieffer to Bose-Einstein condensation and the unitary Fermi gas, *Annu. Rev. Condens. Matter Phys.* 5 (2014) 209.
- [93] P.B. Pipes, Experimental determination of the temperature dependence of metallic work functions at low temperatures, U.S. Dept. Energy 1980 Report No. DOE/ER/02314-16.
- [94] J.G. Daunt, E. Lerner, Adsorption of ^3He and ^4He on copper and on argon-coated copper below 20 K, *J. Low Temp. Phys.* 8 (1972) 79.
- [95] G.G. Kleiman, U. Landman, Theory of physisorption: He on metals, *Phys. Rev. B* 8 (1973) 5484.
- [96] G. Vidali, G. Ihm, H.-Y. Kim, M.W. Cole, Potentials of physical adsorption, *Surface Sci. Rep.* 12 (1991) 133.
- [97] F. Pollock, H. Logan, J. Hobgood, J.G. Daunt, Measurement of molecule-surface binding energies by a time-of-flight diffusion method, *Phys. Rev. Lett.* 28 (1972) 346.
- [98] E.F. Ezell, F. Pollock, J.G. Daunt, Measurements of the binding energies for adsorption of ^3He and ^4He on various substances by dynamic gas diffusion techniques, *J. Low Temp. Phys.* 42 (1981) 47.
- [99] M. Kitajima, K. Shigemura, K. Hosaka, T. Odagiri, M. Hoshino, H. Tanaka, Cross sections for ultra-low-energy electron scattering from atoms and molecules, *AIP Conf. Proc.* 1790 (2016) 020012.
- [100] J.M. Lockhart, F.C. Witteborn, Near zero electric field: free fall of electrons and positrons and the surface shielding effect, in: J.D. Fairbank, B.S. Deaver Jr., C.W.F. Everitt, P.R. Michelson (Eds.), *Near Zero: New Frontiers of Physics*, Freeman, New York, 1988, p. 843.
- [101] W.M. Fairbank, Near zero, a frontier of physics, *Physica* 109 & 110B (1982) 1404.
- [102] D.R. Harshman, A.T. Fiory, Compressed H_3S : inter-sublattice Coulomb coupling in a high- T_C superconductor, *J. Phys.: Condens. Matter* 29 (2017) 445702.
- [103] A. Sanna, C. Pellegrini, E.K.U. Gross, Combining Eliashberg theory with density functional theory for the accurate prediction of superconducting transition temperatures and gap functions, *Phys. Rev. Lett.* 125 (2020) 057001.
- [104] F. Pistolesi, G.C. Strinati, Evolution from BCS superconductivity to Bose condensation: role of the parameter $k_F\xi$, *Phys. Rev. B* 49 (1994) 6356.
- [105] G.C. Strinati, Recent advances in the theory of the BCS–BEC crossover for fermionic superfluidity, *Physica C: Supercond. Applic.* 614 (2023) 1354377.
- [106] H. Dittus, C. Lämmerzahl, Tests of the weak equivalence principle for charged particles in space, *Adv. Space Res.* 39 (2007) 244.
- [107] B. Arneth, Proposed experiment to advance our knowledge on the influence of gravity on elementary particles, *Phys. Essays* 30 (2017) 226.
- [108] V.I. Denisov, I.P. Denisova, M.G. Gapochka, A.F. Korolev, N.N. Koshelev, Gravitational acceleration of a weakly relativistic electron in a conducting drift tube, *Mod. Phys. Lett. A* 33 (2018) 1850192.
- [109] M.P. Gapochka, I.P. Denisova, A.F. Korolev, N.N. Koshelev, E.T. Einiev, On the measurement of the ratio of the gravitational and inertial masses of the electron, *Moscow Univ. Physics Bulletin* 74 (2019) 337.
- [110] P. Touboul, et al. (MICROSCOPE Collaboration), MICROSCOPE Mission: final results of the test of the equivalence principle, *Phys. Rev. Lett.* 129 (2022) 121102.
- [111] E.K. Anderson, et al., Observation of the effect of gravity on the motion of antimatter, *Nature* 621 (2023) 716.

The authors regret that misprints are published in the original version of their article. Corrections are presented as follows:

Citation [20,24] in the next paragraph after equation (1) should be [30,34]. Citation [79] in the paragraph preceding section 3.3.1. should be [99]. In the second paragraph after Fig. 5, the exponent -1 at end of the eighth line should be -2 , to read cm^{-2} . In section 3.3.1, the exponent -11 in the third line before the initial paragraph's end should be -10 to read, 10^{-10} . Citation [87] in the paragraph preceding section 3.4 should be [34]. Citation [38] ending the second full paragraph after Table 1 should be [39]. Please note that the value 105 assigned to Ref. [105] is out of numerical order in the text. The publication date of Ref. [18] is 2001. The full subtitle of Ref. [51] is "Measurement, Classical Theories and Quantum Theory" and the publication date is 2019. The publication date of Ref. [78] is 1983. The authors apologize for the inconvenience caused.

Concerning Ref. [89], the authors wish to point out that text is truncated in the right margin of the abstract in the printed publication [Bull. Am. Phys. Soc. 23 (1978) 565]. For our readers' convenience, missing text is restored by the authors in the following rendering, as indicated by wavy underline:

EN 9 Effect of Helium Gas on the Contact Potential of Copper between 2 and 20K.* J.U. Free,** C.D. Dermer, P.B. Pipes, Dartmouth College.--A non-isothermal Volta technique¹ was used to study the temperature derivative of the contact potential of copper between 2 and 20K in the presence of helium gas. The helium gas pressure was varied between 10^{-6} torr and a few mtorr. A sharp change in the contact potential was observed at approximately 4K. The experimental data will be discussed in terms of adsorption models.

* Supported by the Department of Energy

**On leave from Eastern Nazarene College, Quincy, MA

¹D.H. Darling and P.B. Pipes, Physica 85B, 277 (1977)

The direct hyperlinks for certain references in the article are not published online. For readers' convenience, the direct hyperlinks for these articles are presented in Table 1.

Table 1. Reference numbers and the associated hyperlinks to the publications.

Ref.	Hyperlink to reference article	Ref.	Hyperlink to reference article
1	https://doi.org/10.1103/PhysRevB.41.327	63	https://doi.org/10.1103/PhysRevAccelBeams.22.083101
4	https://doi.org/10.1103/PhysRevX.9.031049	64	https://doi.org/10.1063/5.0031568
7	https://doi.org/10.1002/adma.202006124	67	https://doi.org/10.1103/PhysRevB.7.3541
9	https://doi.org/10.1103/PhysRevLett.129.076403	68	https://doi.org/10.1016/0031-9163(64)90672-9
12	https://doi.org/10.1103/PhysRevB.17.1976	69	https://doi.org/10.1103/PhysRevB.27.6691
13	http://www.jetp.ras.ru/cgi-bin/dn/e_019_01_0269.pdf	71	https://doi.org/10.1103/PhysRevB.69.174505
15	https://doi.org/10.1103/PhysRevB.7.1020	72	https://doi.org/10.1103/PhysRevLett.39.1201
16	https://doi.org/10.1116/1.1318710	73	https://doi.org/10.1103/PhysRevLett.42.1165
18	https://doi.org/10.1103/PhysRevB.64.245112	74	https://doi.org/10.1103/PhysRevLett.56.378
19	https://doi.org/10.1380/ejssnt.2004.191	75	https://doi.org/10.1103/PhysRevLett.56.2303
20	https://doi.org/10.1103/PhysRevB.71.104510	76	https://doi.org/10.1103/PhysRevB.40.182
25	https://doi.org/10.1103/RevModPhys.21.185	77	https://doi.org/10.1103/PhysRevLett.10.486
26	https://doi.org/10.1103/PhysRevB.1.4649	78	https://doi.org/10.1103/PhysRevB.27.150
27	https://doi.org/10.1103/PhysRev.168.737	79	https://doi.org/10.1103/RevModPhys.36.225
28	https://doi.org/10.1103/PhysRev.171.1361	81	https://doi.org/10.1103/PhysRevB.65.144511
29	https://doi.org/10.1103/PhysRevB.2.825	83	https://doi.org/10.1103/PhysRevLett.16.308
30	https://doi.org/10.1103/PhysRevLett.19.1049	84	https://doi.org/10.1103/PhysRev.164.608
32	https://doi.org/10.1103/PhysRevLett.38.1011	85	https://doi.org/10.1103/PhysRevB.28.5075
33	https://doi.org/10.1063/1.1686149	86	https://doi.org/10.1103/PhysRev.140.A1197
34	https://doi.org/10.1103/PhysRevLett.38.1220	87	https://doi.org/10.1103/PhysRevB.19.631
36	https://doi.org/10.1103/RevModPhys.64.237	88	https://doi.org/10.1016/0378-4363(76)90022-X
40	https://doi.org/10.1103/PhysRev.151.1067	93	https://doi.org/10.2172/5589369
41	https://doi.org/10.1063/1.1134860	94	https://doi.org/10.1007/BF00655549
42	https://doi.org/10.1103/PhysRevB.17.1934	95	https://doi.org/10.1103/PhysRevB.8.5484
43	https://inis.iaea.org/records/jvdvj-n3f86	96	https://doi.org/10.1016/0167-5729(91)90012-M
47	https://inspirehep.net/files/f55503250f690969aedfda4ceaf9b4f9	97	https://doi.org/10.1103/PhysRevLett.28.346
48	https://inspirehep.net/files/0f7b50c47ec26bed99a50ff199960259	99	https://doi.org/10.1007/BF00116695
50	https://doi.org/10.1007/BF00116988	101	https://doi.org/10.1088/1361-648X/aa80d0
55	https://doi.org/10.1103/RevModPhys.23.203	102	https://doi.org/10.1103/PhysRevLett.125.057001
57	https://doi.org/10.1103/PhysRevLett.80.4741	103	https://doi.org/10.1103/PhysRevB.49.6356
59	https://doi.org/10.1103/PhysRevB.15.1769	104	https://doi.org/10.1016/j.physc.2023.1354377
60	https://doi.org/10.1103/PhysRevB.27.4612	110	https://doi.org/10.1103/PhysRevLett.129.121102
62	https://doi.org/10.1103/PhysRevB.3.1215		